On the Marine Pollution Prevention Associated with Japan-France Collaborative Research

by

Shoichi HARA*, Kazuo HITOMI**, Masahiko SASANO**,

Koh IZUMIYAMA***, Kenkichi TAMURA****, Hiroshi YAMANOUCHI**,

Kunihiro HOSHINO*,Noboru TAGUCHI**, Shotaro UTO***,

Shigeo KANADA***, Haruhito SHIMODA***,

Daisuke WAKO*** and Shigeki SAKAI*****

Abstract

The Memory of Understanding was contracted between Cedre, the Center of Documentation, Research and Experimentation on Accidental Water Pollution in France and Ship Research Institute (SRI) September in 1999. There were 2 seminars related to oil and chemicals pollution response held at Brest and Tokyo in 2000 and 2001 respectively. After these events both countries decided to have a substantial collaboration project. 3 research themes below were agreed as a collaborative project.

(1)   Research on oil discharge in ice covered area
(2)   Research on Optimum Towing Support System and Emergency Towing Database
(3)   Research on heavy oil monitoring by Lidar

In this report those 3 research themes are introduced and elaborated. The behavior of the oil slick under ice-covered area has been experimentally observed. The experimental results were compared with the numerical calculation solving the deformation and movement of the oil slick and it was found that the numerical simulation explains well the behavior of observed oil slick.

The operational evaluation using Optimum Towing Support System (OTSS), which had been developed in the 5 year special project of Ministry of Transport from the fiscal year of 1998 to 2003, could not be done by the French tugboat, but this research has been decided to continue for next three years to the fiscal year of 2007.

The National Maritime Research Institute (NMRI) could participate in the European project, Depol'04, at-sea oil discharge experiment from Japan through Cedre. It was significant to NMRI in the research topic (3) of this project. During the experiment, four wavelength 2-D images of Lidar signals were observed with a target of oil spill and seawater. However, the heavy oil on the sea surface by Lidar observation could not be detected.

*	Marine Pollution Prevention Research Group	(海洋汚染防止研究グループ)
**	Remote Sensing Research Group	(リモートセンシング研究グループ)
***	Ice Engineering Research Group	(氷海技術研究グループ)
****	Deep Sea Technology Research Group	(深海技術研究グループ)
*****	Faculty of Engineering, Iwate University	(岩手大学工学部)

Contents

1. Introduction

Cedre in France means the Center of Documentation, Research and Experimentation on Accidental Water Pollution. Cedre was created in 1976 within measures taken after the wreckage of the oil tanker 'Amoco Cadiz' to improve preparedness against accidental water pollution and strengthen the national response organization. Its expertise encompasses both marine and inland waters.. The oil leakage incident of tanker 'Erika' occurred offshore Brest December in 1999 and it gave a devastating environmental damage to the coast of Biscay Bay. In Japan there was a same oil leakage incident of tanker 'Nakhodka' January in 1997. Both countries had a same experience of response against the heavy oil

leakage. Its common knowledge of oil pollution response should be shared with each other to the further improvement of measures against the disaster.

The seminar titled 'From the Nakhodka to the Erika' was held at Brest July in 2000. Further, the seminar titled 'Getting Better Prepared to Face Offshore Oil and Chemical Spills' was also held at Tokyo October in 2001. Both seminars were successful and their purpose to hold an each seminar was fully achieved After these events both countries decided to have a substantial cooperative project. 3 below research themes were accepted by both countries.

(1) Research on oil discharge in ice covered area

(2) Research on Optimum Towing Support System

and Emergency Towing Database

(3) Research on heavy oil monitoring by Lidar

In this report those 3 research themes are introduced and elaborated. Especially the Depol'04, at-sea oil discharge experiment is the European project, the participation in the European project from Japan through Cedre was significant to NMRI because the field test discharging the real oil is prohibited in Japan. National Maritime Research Institute (thereafter termed NMRIin this paper) has obtained the data using Lidar instrument in the field test.

Cedre is interested in the marine pollution of Arctic region and agreed to cooperate in exchanging the information. As for the research item (2), the captain of the tugboat rented by the government at port of Brest was supposed to cooperate in the operational evaluation of the Optimum Towing Support System (OTSS). OTSS was developed by NMRI in a 5 year special research project sponsored by the Ministry of Transport from the fiscal year of 1998 to 2002. The model experiment and field test have been carried out to validate the element technology of OTSS. NMRI would like Cedre to utilize the tool of OTSS for the drift prevention of disabled ships which have a possibility to cause another accident. The operational evaluation has also been planned to cooperate with the Japan Coast Guard in 2005. After the operational evaluation results were stored the emergency towing database will automatically be produced.

2. Research on Spilled Oil Behavior in Ice-covered Waters

2.1 Introduction

With the increasing demand for energy resources, activities of the petroleum exploitation have been expanded its area to the "frontiers" such as ice-covered waters and deep sea areas. First attempts for the petroleum development in the ice-covered water were made in the 1980s in the Arctic sea areas including the Beaufort Sea and High Arctic Islands[1). Great amount of activities was made for the exploration of oil and gas in these areas. However harsh conditions in the Arctic required high technology that is totally different from that for regions with moderate conditions, and made the development economically infeasible.

Today petroleum resources in ice-covered waters are regaining attention as new sources for energy supply. This time developments have shifted to the areas with relatively mild conditions. One of such areas is the continental shelf of the Sakhalin Island, Russia, which is located just north of Hokkaido, the northernmost island of Japan. In Sakhalin II, one of oil fields set out in the water around the island, commercial production of oil had already started in 1999. Petroleum development in the offshore Sakhalin is expected to be new and large energy resource for Japan, which lacks domestic resources and rely on the importation for most of the energy supply. There is growing apprehension, on the other hand, of marine pollution due to accidents in the production and transportation of oil.

Special concern is attended to the possibility of oil spilling in ice-covered conditions. The Sea of Okhotsk, where Sakhalin and Hokkaido Islands face, is known to be the southernmost sea area that sees sizable amount of sea ice in winter. In the northern Sakhalin sea ice presents for about six months and in Hokkaido for about two months. The presence of ice makes the behavior and fate of spilled oil totally different from those in open water conditions. However, there have been only a limited number of studies on the oil spilling in ice-covered waters.

In view of the situation NMRI has been studying the problems related to oil spilling in ice-covered waters. There are three issues that the study has focused on; they are; the behavior of spilled oil in ice-covered waters, interaction of oil with ice, and the recovery of oil in ice. This report presents the results of the study on the first issue.

2.2 Research outline

There are many aspects to be studied on the behavior of oil spilled in ice-covered waters. This study focused on the spreading and drifting behavior of oil spilled under an ice cover. There can be various scenarios for the oil spilling in ice-covered waters. From the pollution prevention viewpoint, one of the most difficult situations is the oil being spilled under a continuous ice cover. One of possible scenarios that could cause such a situation is oil spilling from underwater pipelines, which are planned to be built in the Sakhalin offshore fields. Oil spilled in water under an ice cover will spread along the underside of the ice. It is very difficult to locate such oil, which is of the first and foremost importance for the pollution prevention operation. However, there have been only a limited number of studies done on the spreading behavior of oil under an ice cover. Oil slick under ice may drift by current in water. This is also an important issue from the pollution prevention viewpoint but poorly studied.

This study was done as a joint research between

NMRI and Iwate University. NMRI studied the behavior of oil under ice by way of experiment in a model test basin. Iwate University conducted numerical simulation for the phenomena.

2.2.1 Experimental Study

The experiment was performed at NMRI's ice model basin. Fig. 2.1 shows a cross section of the facility. The basin is 35 m in length, 6 m in width and 1.8 m in depth and housed in a cold chamber. Air temperature inside the chamber can be lowered to –20 degrees C to grow ice in the basin. Below the basin is a basement. There are observation windows on a sidewall and bottom of the basin.
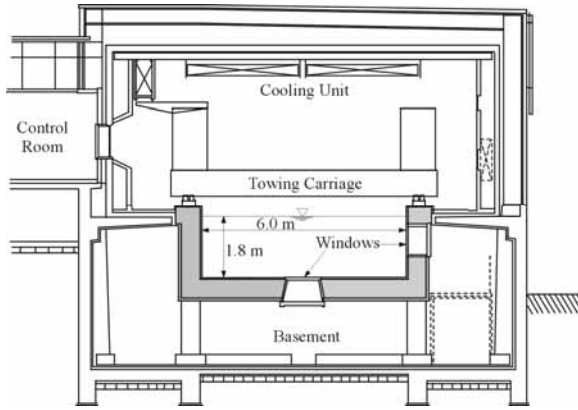

Fig. 2.1   Cross Section of NMRI Ice Model Basin

Two series of experiments were performed. The first series of experiments were performed to study the spreading behavior of oil spilled under an ice cover. In the experiment oil was spilled from a point source in water covered by ice (see Fig. 2.2). Oil then rose to the ice and spread along the ice-water interface. The spreading behavior of the oil was recorded by VTR cameras placed on the ceiling of the basin room and under an observing window in the bottom of the tank. The second series of experiments were performed to study the drifting behavior of oil spilled under an ice cover by water current in the water. In this experiment oil was spilled under an ice floe cut out in the basin(Fig. 2.3). The ice floe was then pushed at a constant speed by the carriage of the basin. A VTR camera set above the ice floe recorded the drifting motion of the oil relative to the ice floe.

A machine lubrication oil was used for both tests. Density and viscosity of the oil were 890 kg/m^3 and 0.123 Pa-sec at 0 degree-C, respectively. The oil was colored dark blue for better observation by cameras.

Freshwater ice was used for the tests. The ice is transparent and allowed good visibility of oil through it.
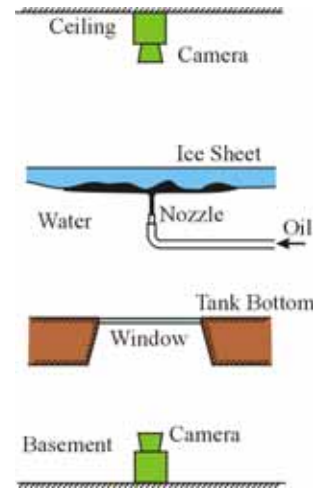

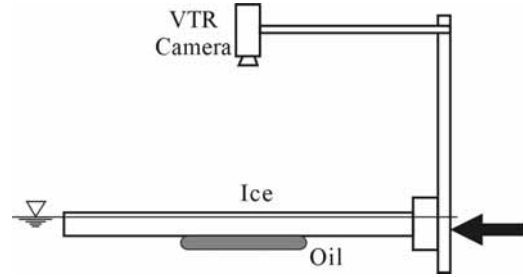Fig. 2.2   Schematic View of Oil Spreading Test

Fig. 2.3   Schematic View of Oil Drifting Test

2.2.2 Numerical Simulation

Iwate University worked on the numerical simulation for the spreading and drifting of oil under an ice cover. The governing equations for the phenomenon are the Navie-Stokes' and the continuity equations. It was assumed that the velocity of oil in the vertical direction (z-direction) is negligibly small compared with those in the horizontal directions (x- and y-directions) and can be ignored. The equations were then integrated in the vertical direction over the thickness of the oil layer to obtain the two dimensional equations as;

$$\frac{\partial h}{\partial t} + \frac{\partial M}{\partial x} + \frac{\partial N}{\partial y} = 0$$

$$\frac{\partial M}{\partial t} + \frac{\partial}{\partial x}(uM) + \frac{\partial}{\partial y}(vM) = -gh\frac{\partial H}{\partial x} - \frac{f_x}{\rho} \quad (2.1)$$

$$\frac{\partial N}{\partial t} + \frac{\partial}{\partial x}(uN) + \frac{\partial}{\partial y}(vN) = -gh\frac{\partial H}{\partial y} - \frac{f_y}{\rho}$$

In the equations, u and v are velocity in the x- and

y-directions, h and H are the thickness and depth of underside of the oil layer, g and ρ are acceleration due to gravity and oil density, respectively. M and N are flow fluxes and f_x and f_y are external forces on a unit length in the x- and y-directions, respectively.
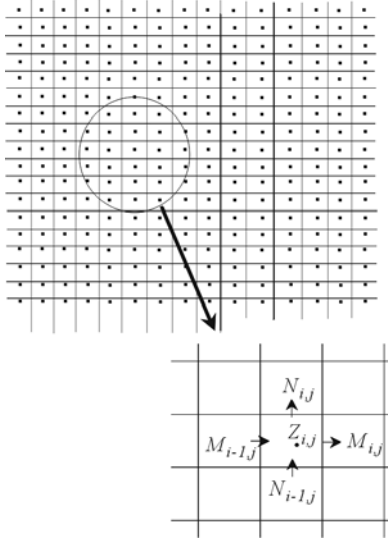

Fig. 2.4　Schematic Explanation of Computation

In the computation the equation (2.1) is formulated in a staggered difference scheme in space and leap-frog difference scheme in time. Computation was made in the following procedure.

1. Divide the computation area into the rectangular grids as shown in Fig. 2.4,
2. Give the depth of the underside of the ice cover at the center of each grid,
3. Give the oil outflow at a grid point, and
4. Calculate the flow flux and oil thickness.

The external forces taken into account in the computation include the form drag force, shear force and surface tension force. It was assumed the form drag force could be negligibly small for the case of oil spreading under the ice. This is because that the spreading speed of oil, namely the speed of the edge of oil layer, is low except for very initial stage of oil spreading[2]. The shear force was assumed to be in proportion to the second power of the oil speed.

For the determination of interfacial tension force, the result of study by Konno[3] was used. The interfacial tension force is one of forces that govern the spreading behavior of oil. There are three kinds of interfaces at the outer edge of an oil slick under an ice cover, they are oil-water, oil-ice and water-ice interfaces. The net interfacial tension force is given as the sum of tension forces on these interfaces, and acts as a retarding force

to the oil spreading. Konno by theoretical consideration and experiment showed that the net interfacial tension force acting on an oil slick under an ice cover with a flat and horizontal underside is given by twice the value of the oil-water interfacial tension force. This is an important finding for the study of oil spreading under ice, as it is technically difficult to determine the values of the other two interfacial tension forces.

2.3 Results and Discussion
2.3.1 Spreading of Oil under Ice

One of the most important factors that influence the spreading behavior of oil under an ice cover is the underside configuration of the ice. Field measurement at the Sea of Okhotsk showed that the underside of sea ice is rarely flat and has roughness of various size[4]. The present study focused on the effects of the roughness in the underside of ice cover on the spreading of oil.

(a)　Ice Cover with a flat and horizontal Underside
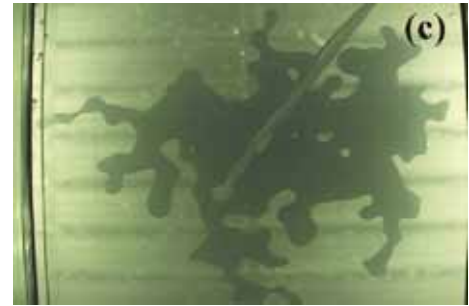
(b)　Ice Cover with a Roughened Underside

Fig. 2.5　　Pictures of Oil Spreading under an Ice Cover

In the experiment at NMRI's ice model basin tests were performed for various underside configurations of ice including the flat and horizontal one as a basis of the study. Fig. 2.5 shows examples of pictures taken by a camera under a bottom window showing the oil spreading under an ice cover with a flat and horizontal underside (Fig. 2.5 (a)) and an ice cover with an uneven underside with roughness (Fig. 2.5 (b)). It is seen that the spreading behavior of oil is totally different between the two cases. For the flat and horizontal underside oil

spreads over a circular area, while it is very irregular shape for the uneven underside.

The underside configuration of the ice cover affects the area of oil under the ice as well as the shape of slick. Fig. 2.6 shows the effect of the underside roughness on the area of oil slick. In the figure A_R and A_L are oil area under an ice cover with a roughened underside and a flat and horizontal underside, respectively, and R_S is the height of roughness, which was in this study defined by the standard deviation of the underside profile of the ice. It is seen that the ratio A_R/A_L decreases as the roughness height increases. This means that the area of oil slick under an ice cover decreases as the size of the roughness.
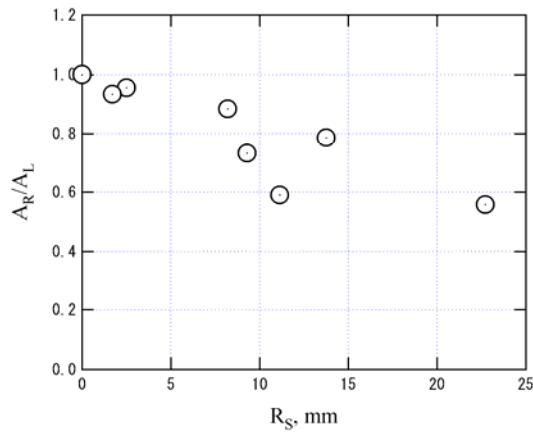

Fig. 2.6   Correlation of Oil Area and
Roughness Height

In parallel to the experiment a computer program of the numerical simulation was developed at Iwate University. The simulation was validated by comparing with the results of the experiment. For the validation detailed measurements of underside configuration of ice was performed for selected cases of the experiment. Fig. 2.7 is an example of the result of such a measurement. The measured data was used as an input data set for the computation.

Figure 2.8 shows a comparison of observed and simulated oil slick shape. Although there are some discrepancies between the two results, oil slick shapes in general are very similar. Fig. 2.9 shows a comparison of measured and simulated oil slick area. It can be seen that the simulation gives lager oil area for the cases with the flat and horizontal underside of ice, while it gives smaller area for the uneven underside cases. However, the difference is insignificant. Again there is a very good agreement between the experiment and

simulation. From those results it was concluded that the present numerical simulation was validated by the experimental results.
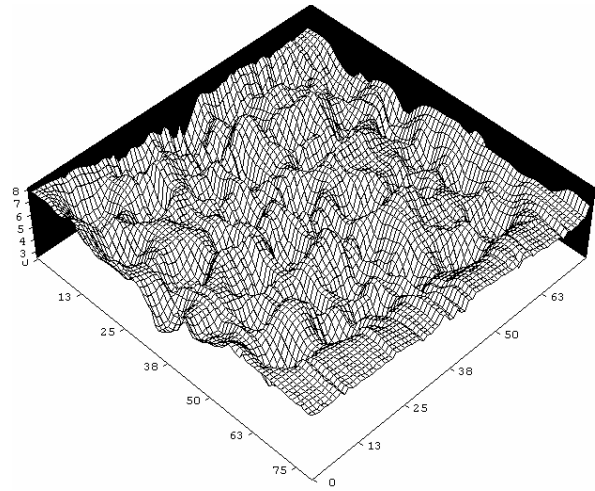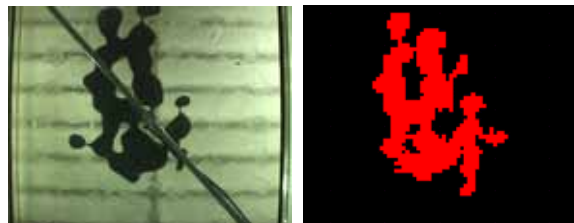

Fig. 2.7   An Underside Configuration of Ice for
an Oil Spreading Test

240 seconds after the Onset of Spill

480 seconds after the Onset of Spill

720 seconds after the Onset of Spill
Experiment   Simulation

Fig. 2.8   A Comparison of Observed and
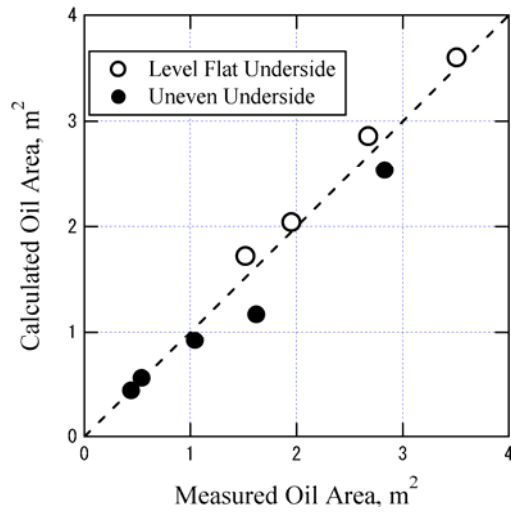Simulated Oil Slick Shape

6

Fig. 2.9   A comparison of measured and simulated oil slick area

Following the validation of the simulation by experimental results, computation was made to simulate the oil spreading behavior under the full-scale conditions. The full-scale simulation was made for the condition of a 5,000 m^3 of oil was spilled from a point source under an ice cover at a rate of 0.5 m^3/sec for a period of 10,000 seconds (2.78 hours). The properties of the oil were assumed to be the same as those of the oil used for the experiment. They were well within the range of values for crude oils.

The simulation was made for the underside configuration of ice that was virtually created using the results of field measurement performed at the Sea of Okhotsk[5]. Fig. 2.10 shows the results of the field measurement. Fig. 2.10 (a) shows the normalized (divided by the squared standard deviation) power spectrum density curves obtained from the field measurements. The gray lines show the data from individual measurements and the solid line is the average line for those measurements. Although there is some scatter between the lines for individual measurements, the general trend is well given by the average line. In the simulation the normalized power spectrum density curve given by the average line was used to create the virtual underside configuration of the ice.

On the other hand Fig. 2.10 (b) shows that the standard deviation varies widely from data to data. Some data show a very small standard deviation indicating fairly smooth underside of ice, while some show large value indicating very deformed ice. In the simulation calculation was made for the five different

values of standard deviation of R_s=0.10, 0.25, 0.50, 1.00 and 1.50 m.
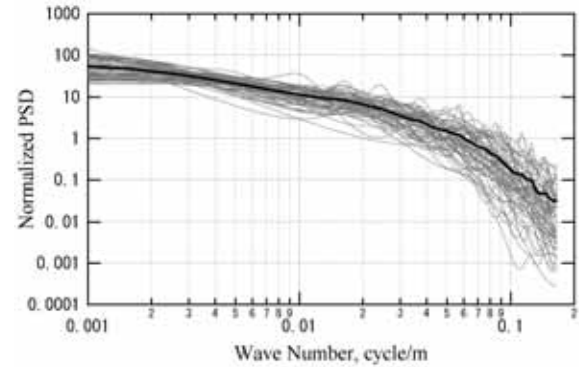
(a)   Normalized power spectrum density function
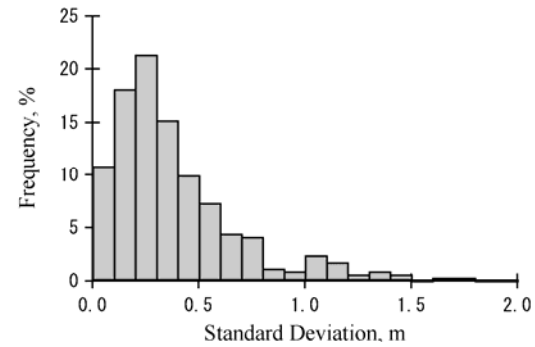
(b)   Histogram of standard deviation

Fig. 2.10   Results of field measurement for underside configuration of sea ice
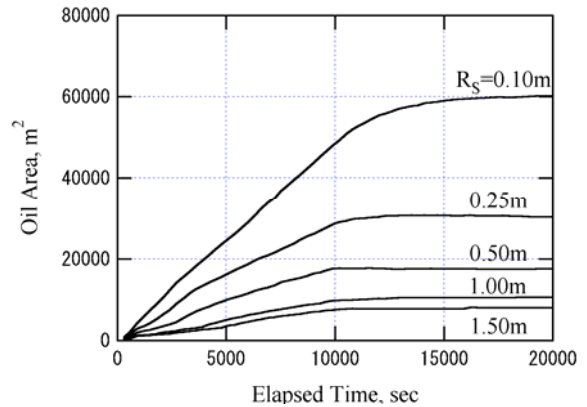
Fig. 2.11 Results of full-scale simulation

Figure 2.11 shows the results of the full-scale simulation. It is clearly seen in the figure that the oil slick area decreases as the size of underside roughness of ice cover increases. It is also seen that the oil area continues grows even after the termination of oil spilling (at 10,000 sec) in the cases with small under-ice roughness, while it soon levels off for the large roughness cases.
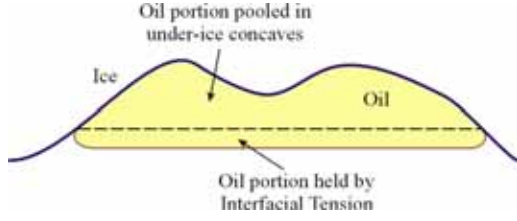
Fig. 2.12 Two mechanisms to hold oil under ice

It has been shown that the size of under-ice roughness has great effects on the spreading of oil under an ice cover. It was attempted to create a theoretical model to explain it. In the model two kinds of mechanisms to hold oil under an ice cover were considered. Fig. 2.12 schematically explains the two mechanisms. One mechanism is the oil pooling in concaves in the underside of the ice. This causes the decrease of oil slick area with the increase of the size of under-ice roughness as shown in Fig.s. 2.6 and 2.11. The other mechanism is the interfacial tension force acting on the outer edge of the oil slick. As previously described, the net interfacial tension force acts as a retarding force to the oil spreading under an ice cover. This force holds oil under the oil hold in the under-ice concaves (see Fig. 2.12) It is assumed that the thickness of this oil layer is the same as that of oil slick under an ice cover with a flat and horizontal underside. Yapa[6] gave the following equation for this thickness, h_T.

$$h_T = \sqrt{\frac{2\sigma_N}{\Delta\rho g}} \,, \qquad\qquad (2.2)$$

where $\Delta\rho$ is density difference between water and oil and g is the acceleration due to gravity and σ_N is the net interfacial tension force.

The total volume of oil is given as a sum of the two oil portions as

$$V = A_R\left(h_C + h_T\right), \qquad\qquad (2.3)$$

where h_C is the average thickness of oil pooled in the under-ice concaves. For the same volume of oil spill under an ice cover with the flat and horizontal underside, we can write

$$V = A_L h_T \,. \qquad\qquad (2.4)$$

Equations (2.3) and (2.4) yield

$$\frac{A_R}{A_L} = \frac{1}{h_C/h_T + 1} \,. \qquad\qquad (2.5)$$

It is reasonable to treat the average oil thickness, h_C,

pooled in the under-ice concaves as a function of the size of under-ice roughness. If we assume a linear correlation between the two as,

$$h_C = C R_S \,, \qquad\qquad (2.6)$$

where C is a constant, equation (2.5) can be rewritten as

$$\frac{A_R}{A_L} = \frac{1}{C(R_S/h_T) + 1} \,. \qquad\qquad (2.7)$$

Equation (2.7) gives the oil slick area, A_R, under an ice cover with the under-ice roughness of the size of R_S, as the values of h_T and A_L can be calculated from equations (2.2) and (2.4).

Equation (2.7) was compared with the results of experiment and simulation to check the validity of the model. Simulation was made for the virtual under-ice configuration used in the full-scale simulation and for oil properties as shown in Table 2.1. In the table ρ_O is the oil density. h_T, is an important parameter of the model. As seen in Table 2.1 simulation covers a wide range of h_T from 2.8 mm to 13.6 mm.

Table 2.1 Oil Properties used for Simulation

	ρ_O kg/m^3	σ_N mN/m	h_T mm
Oil-1	890	45.4	9.18
Oil-2	890	20.0	6.09
Oil-3	890	7.5	3.73
Oil-4	800	45.4	6.81
Oil-5	800	20.0	4.52
Oil-6	800	7.5	2.77
Oil-7	950	45.4	13.61
Oil-8	950	20.0	9.04
Oil-9	950	7.5	5.53

Figure 2.13 shows correlation of relative oil area, A_R/A_L, and relative roughness height, R_S/h_T, calculated from the results of simulation and laboratory test. The curve in the figure shows theoretical correlation given by equation (2.7) with a constant of $C = 0.5$. Although there are some discrepancies between the theoretical curve and simulation and laboratory test results, equation (2.7) well explains the general trend through the two kinds of data.

In Fig. 2.13 there are three regions. In the region of small roughness height, say $R_S \le h_T$, there is only minor dependence of oil area on the size of under-ice roughness. In this region interfacial tension is the dominant mechanism to hold oil under the ice. As the size of

under-ice roughness increases, its effect becomes dominant. In the region of large roughness height, say $R_S \geq 50 h_T$, there is nearly an inverse correlation between the oil area and the roughness size. In this region pooling is the dominant mechanism to hold oil under the ice. If R_S is much greater than h_T, we will have the following equation for this region,

$$A_R = \frac{2V}{R_S},\qquad\qquad (2.8)$$

which is shown in the broken line in Fig. 2.13. Equation (2.8) can be useful for a rough estimation of oil area in field conditions. There is a transition region between the above-mentioned two regions.
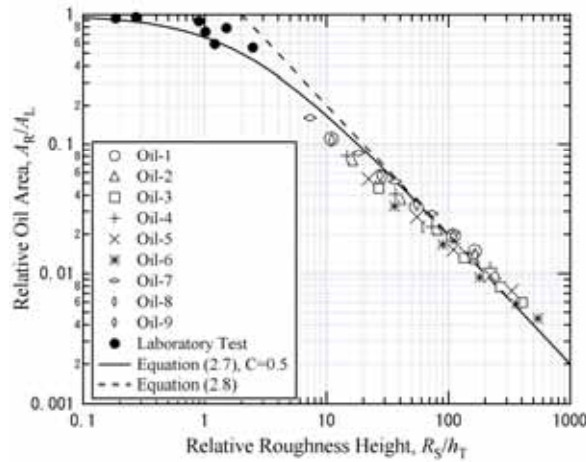

Fig. 2.13   Comparison of equations (2,7) and (2.8) with laboratory test and simulated results

As a conclusion it can be said that theory given by equation (2.7) gives a reasonable explanation on the effects of two mechanisms to control the area of oil under an ice cover. There still is, however, a point that requires further study. That is the assumption given by equation (2.6). The equation gives a linear correlation between the pooled oil thickness and the size of under-ice roughness. As can be seen in Fig. 2.13 a constant $C = 0.5$ gives a good agreement between the theory and test and calculation results. This means that half the size of the standard deviation of under-ice roughness contributes to the pooling of oil. There is not, however, a physical explanation on the validity for $C=0.5$. More detailed studies are needed on the effect of under-ice roughness on the oil storage capacity of the ice.

2.3.2 Drifting of Oil under Ice

Oil drifting tests were performed for ice floes with a flat and horizontal underside. In the test it was observed that oil slick under the ice, which was initially of a circular shape, was deformed by current against it. Fig. 2.14 shows examples of observed oil slick deformation for a low and high current speed cases. In the low speed test the oil slick gradually elongated to the lateral directions to the current to form a crescent-like shape. At the higher speed although the slick shape is more rugged and there is some oil separation, the general deformation pattern is similar to that at the lower speed.
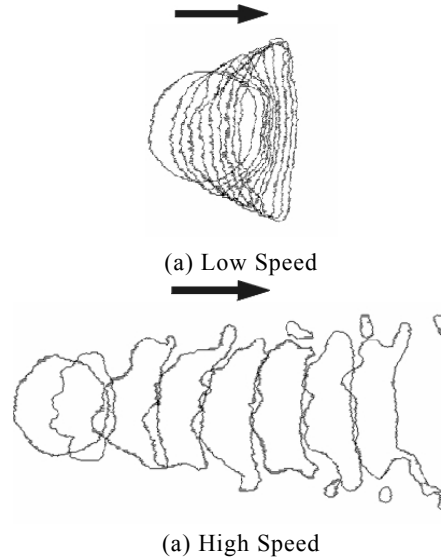

(a) Low Speed

(a) High Speed

Fig. 2.14   Examples of oil slick deformation by current

In the drifting test it was observed that the front edge of the oil slick is thickened while the region behind it remained unchanged. The thickening of the oil layer was considered to be a key phenomenon in the drifting of oil under ice. It was then attempted to measure the front edge thickness of oil in current. In the test two volumes of oil were used – 2L and 4L. The oil was put in a channel made of two vertical ice slabs attached under an ice sheet. The ice sheet was then towed at a constant speed. The test was made for two cases with and without an oil stopper at the end of the channel. In the test underwater observation of oil deformation was made using a VTR camera.

Figure 2.15 is an example of pictures taken by the VTR camera. In the picture the profile of the oil and underside of the ice are enhanced. It is seen that the front edge of the oil is thickened due to current. The tests were made for various speed of ice floe and the thickness of oil front edge was measured from pictures as shown in Fig. 2.15. Fig. 2.16 shows the result of the measurement. The figure shows that there is a very good

linear correlation of the front edge thickness of oil slick with the current speed squared. Oil slick thickness under the no current condition is 10 mm. Fig. 2.16 shows the oil thickness in the region of low current speed approaches this value. There is practically no effects of the oil stopper on the front edge height of the oil.
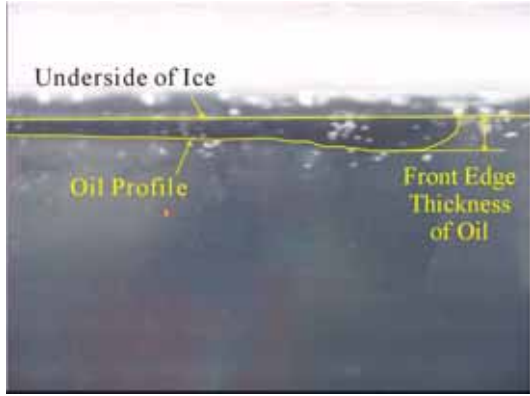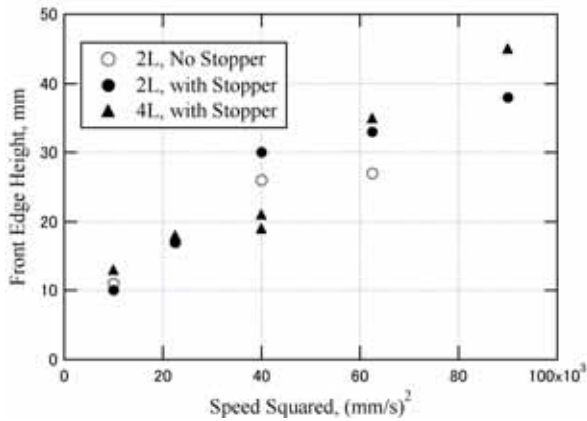

Fig. 2.15 Oil Profile in Current

Fig. 2.16   Results of Front Edge Height Measurement

The drifting of oil under an ice cover was studied by numerical simulation as well. In the computation the effects of oil layer thickening was taken into account. The thickening of oil can contribute to the drifting in two ways. Fig. 2.17 schematically explains the two effects. One is the internal flow of oil. The thickening of the front edge unbalances the pressure in the oil slick, which causes the internal flow of oil from the front region to the aft-region. This results in the drifting of oil slick as a whole. The other effect is the increase of form drag force acting on the front edge of the slick. In the simulation the first effect was taken into account. Experimental data shown in Fig. 2.16 is used in the simulation.
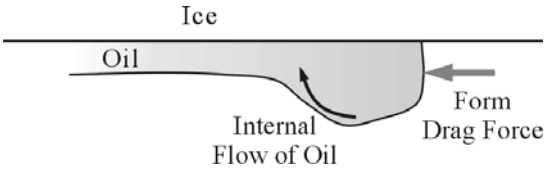
Fig. 2.17   Schematic Description of the Oil Thickening Effects on Oil Drift
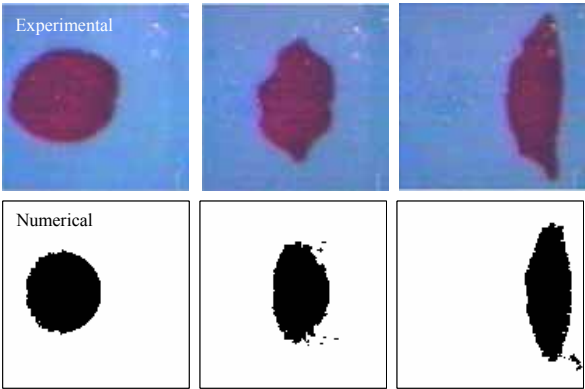
Fig. 2.18   Comparison of observed and calculated oil slick shapes
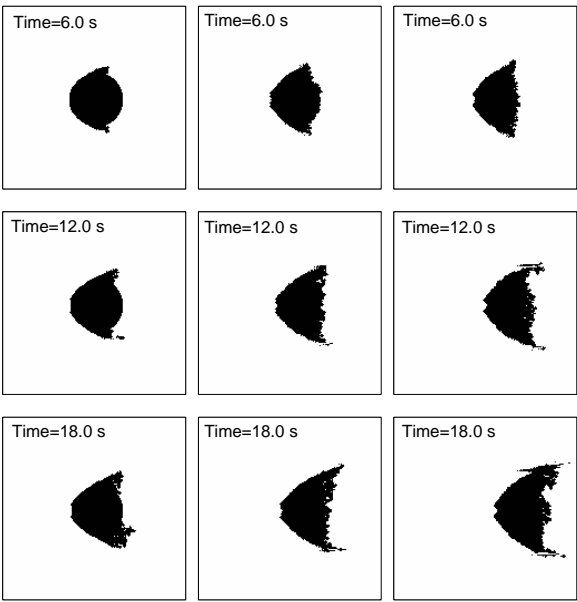
(a) 40 mm/s   (b) 80 mm/s   (c) 120 mm/s

Fig. 2.19   Calculated oil slick shapes at different current speed

Fig. 2.18 shows a comparison of the experimental observation and the results of the numerical calculation. In the Fig. there is a current from the left to the right. It is seen that the calculated deformation process of the oil

slick well explains that observed.

Fig. 2.19 shows examples of calculation results of oil slick deformation process at different speed of 40, 80 and 120 mm/s. In the figure it can be seen that the drifting speed of the oil increases with the increase of current speed. It is also seen that the oil slick deforms from the circular shape to the crescent-like shape as the time goes. This deformation is more distinct at the higher current speed.

2.4 Conclusion

This report presented the results of a study on the spreading and drifting of oil spilled under an ice cover. The study was conducted as a joint research between NMRI and Iwate University. In NMRI experimental study was performed and Iwate University conducted numerical simulation. Behavior of oil spilled in ice is an issue that has not yet been well understood. However, considering the rapid progress of petroleum development in offshore Sakhalin, it is a matter of great urgency for Japan to have appropriate understanding of the phenomenon. It is hoped the findings obtained in the present study could contributed future studies in this field.

References

1) Frederking, R., 1994. A Review of Cold Region Developments in Canada. *Proceedings of the 4th International Offshore and Polar Engineering Conference*, Vol. 2, pp. 414 – 421.

2) Izumiyama, K, Uto, S, Narita, S, and Tasaki, R, 1998. Effects of Interfacial Tension on the Spreading Behavior of Oil under and Ice Cover. *"Ice in Surface Waters,"* Shen (ed.), Vol 1, pp 419-426.

3) Konno, A. and Izumiyama, K. On the relationship of the oil/water interfacial tension and the spread of oil slick under ice cover, *Proceedings of 17th International Symposium on Okhotsk Sea & Sea Ice*, 2002, pp 275-282.

4) Yamamoto, Y., Sakikawa, M., Honma, D. and Kioka, S., 2002. Underside Profile and Drift Characteristics of Sea Ice in the Japanese Coast of Okhotsk Sea. Ice in the Environment, *Proceedings of the 16th International Symposium on Ice*, Vol. 2, pp. 399 – 406.

5) Yamamoto, Y., 2003. Study on the Sea Ice Conditions at the Sea of Okhotsk, *Project Report for "Fundamental Study on Behavior and Recovery of Spilled Oil in Ice-covered Waters"* (in Japanese).

6) Yapa, P, and Chowdhury, T. "Oil Spreading under Ice Covers." *Proc the Eleventh International Oil Spill Conference,* 1989, pp 161-166.

3. Research on Optimum Towing Support System

3.1 Introduction

The 5 year research project from the fiscal year of 1998 to 2002 named 'Drift prevention of disabled ships in rough seas' sponsored by the Ministry of Land, Infrastructure and Transport finished in March 2002. The purpose of this project is to establish the technology to prevent disabled ships caused by the engine trouble and so on from drifting and to tow them to the safety area, and thus the secondary disasters would be prevented from occurring. The Optimum Towing Support System called OTSS using the personal computer has been developed[1),2),3)]. It can provide the operators with the information of prediction such as drift motion, towline tension, maneuvering and needed horse power of the tugboat. The outline of the system and the description of the instruction manual of the system for the practical operation using the monitor display of the computer are introduced.

3.2 Outline of OTSS

OTSS is the computer program which can predict the drift motion, towline tension, unstable motion of towed ships and towing trajectory using the personal computer. The function of the system is shown in Fig. 3.1.

(1) Similar ship production function

The kinds of type ships for shipwrecks are shown in Table 3.1. The various data of shipwrecks can be calculated by making input of the loading condition and main particulars such as length, breadth and depth.

1) Similar ship type

The similar ship offset can automatically be

Table 3.1　Main particulars of type ships.

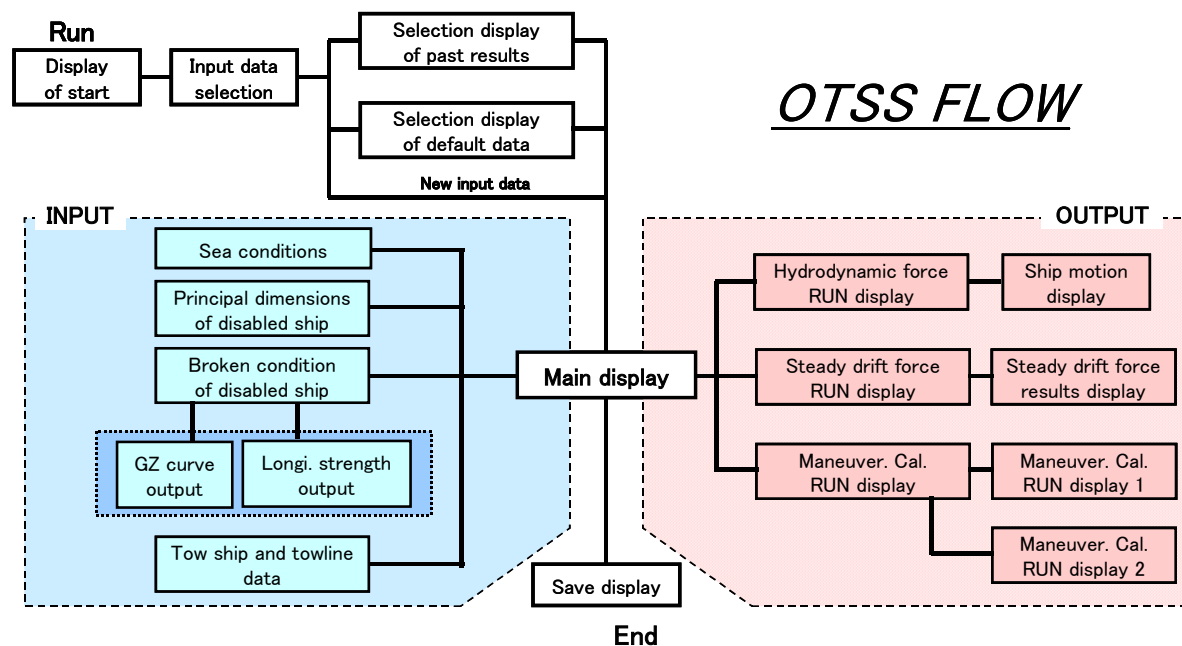| Type ship D/W	Tanker 1 258000	Tanker 2 150000	Container 23700	Barge	PCC 12500	Cargo 18000	Fishing boat 499GT
L_{PP} (m)	320.00	265.00	200.00	70.00	180.00	156.00	53.00
B (mld) (m)	58.00	48.30	32.00	20.00	32.00	26.60	9.40
D (mld) (m)	28.80	22.40	16.50	4.00	14.00	14.10	3.95
d (mld) (m)	18.50	15.20	10.50	3.80	8.50	9.00	3.60
Cb	0.83	0.83	0.56	0.92	0.55	0.70	0.66
lcb (%)	−3.70	−3.30	2.40	−0.90	2.38	−0.54	1.15
	single hull	double hull					

Fig. 3.1　Flow of OTSS

produced using the dimension of length L, breadth B and depth D of type ship shown in Table 3.1.

2) Compartment

The transverse coordinate of ship structure can be converted by the ratio of breadth to depth. The distance from the hull is done by the same manner. The frame number of ship structure is not changed and only the frame space is changed.

3) Light weight

Basic weight, local weight and loading condition can be calculated by multiplying the ratio of L'B'D'/(LBD). The local weight means the partial load such as engine part and deckhouse out of dead weight. L', B' and D' indicates the dimension of towed ship.

(2) Input of upper-structure on the deck

The wind resistance of towed ships above the sea, hydrodynamic resistance and wave drift force below the sea surface can be calculated by making input of geometric shape such as cylinder and rectangle on the deck.

(3) Calculation function of center of gravity

The center of gravity can be calculated and it is used for calculation of ship status and damage stability.

(4) Mesh generation function for calculating wave drift force

The mesh on the ship hull can be generated and that on the submerged part can be output on the display.

(5) Final ship status calculation function (damage stability calculation function)

Calculating the damage stability by making input of the kind of type ship, loading condition and main particulars of dimensions, the final status of the towed ship can be estimated.

(6) Stability calculation function on the capsized and broken condition

GZ curve(refer Fig. A13,GZ:stability lever) and final equilibrium condition defined by trim, heel and mean draught by the damage stability on the capsized and broken condition can be calculated. When the ship is broken, the broken tank can automatically be detected considering the broken position.

(7) Longitudinal strength

The shearing force and bending moment along the length can be calculated.

(8) Hydrodynamic force and ship motion

The hydrodynamic force such as added mass force, wave damping force and wave exciting force, ship motion and wave drift force can be calculated[4),5).6)]. Further, 3-D ship animations at various wave incident angles can be observed[7)].

(9) Steady drift motion [8)]

Calculating the hydrodynamic resistance, wind resistance, wave drift force and current resistance during tow, the steady equilibrium equation can be solved. The bow direction, drift speed and drift direction can be obtained. The number of the solution can be multiple in some cases.

(10) Maneuvering simulation[9),10),11)]

The maneuvering simulation in the tow and towed ship system can be carried out. The coefficients used for this simulation can automatically be obtained from the experimental data using the patrol boats models, existing experimental formulae and the database of hydrodynamic forces developed by the National Maritime Research Institute and thus the maneuvering equation can be solved.

The behaviors of the towed ship such as the unstable motion and trajectories of tow and towed ship can be calculated in the time domain.

3.3 Issue of OTSS

OTSS has been developed for the disabled ships which was damaged or broken due to marine accidents. However, this computer simulation program for those disabled ships has a limitation to apply to the towing operation on site. This application limitation is described below.

(1) Towing speed

As the wave drift force is calculated on the assumption that towing speed is zero, its effect on the wave drift force cannot be ignored when the towing speed becomes large. The towing speed larger than 5 kt is considered to have a certain effect on the estimation of the hydrodynamic force.

(2) Effect of ship status

When the ship has a large trim or heel, it is difficult to estimate the wind pressure coefficients. Those can be calculated only on the even keel condition at the moment. The data for every type ship are already stored as a database on the even keel condition.

(3) Effect of ship form

When the ship is broken, it is quite difficult to estimate the hydrodynamic coefficients. The prediction of the maneuvering performance such as longitudinal force and moment has a problem on the accuracy. Therefore, the estimation accuracy of maneuvering performance for the arbitrary form

floating objects is limited. The accumulation of database can improve this defect.

(4) Rudder performance

The single rudder performance is applied to the estimation of twin rudder performance using the full-scale results of turning performance test. Those coefficients are used in the maneuvering equation.

(5) Towing point

Maneuvering simulation on bow tow can be done easily, but that on stern tow has a problem on the accuracy. There are very few experimental coefficients for backward maneuvering and thus it is quite difficult to estimate the ship behavior although the developed database of hydrodynamic forces is used in the system. The numerical calculation computer program has been developed for the trimmed ships but not for the heeled ships.

3.4 Emergency towing database

The ship data can be registered in the OTSS system in advance. If the rescue organization can keep the needed ship data, the shipwrecks would have a possibility to be surely rescued. Thus the disastrous marine accident could have been avoided. This leads to the higher rescue probability if the ship data was in advance registered in the database of the rescue organization. If this operational system is adopted by the rescue organization under the umbrella of international organization such as IMO, the OTSS system would be much useful tool.

When this system is used on site, the simulation results are first produced in order to estimate the towing behavior of the towed ship. Then the operational data are produced at the same time by the data input of towing event and can be compared with the simulation results. Thus the towing database can actually be constructed. This database will be useful for the rescue organization in the world.

The computer simulation of the behavior of the towed ship needs the following data of the tugboat. Fig. 3.2 shows the test results for controllable pitch propeller. CPP blade angle, engine output, propeller slip ratio are shown in the figure. The principal particulars for the propeller are also needed. The diameter, blade number, pitch ratio, expanded blade area ratio, output power of engine, engine reduction number and propeller reduction number are the data of propeller. As for the maneuverability of the tow ship, the maneuvering characteristics such as transfer and advance are needed for the estimation of the towing of the tugboat.

The following items are needed for the tow and towed ship. Name of towed ship, area of sea, date, place, weather, sea condition, motion of towed ship, principal dimension of towed ship, engine condition of towed ship, horse power, ship speed, propeller data
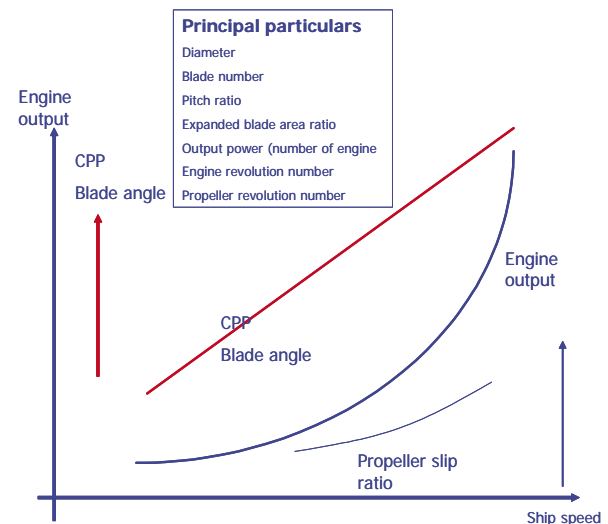

Fig.3.2　Tests results for controllable pitch propeller with constant revolution

Table3.2 Retrieval items of the emergency towing database

No.	Term of towing		Towed ship		Are of towing							Name of tugboat						Name of the person			
													tow ship					towed ship			
area of sea	date time	position	distance of sail	time of sail	mean speed	wind direction wind force	wave current	$\alpha°$	$\beta°$	weather	propellea		horse power	touline tension	length of towline	length of anchor chain	draft	displace-ment	engine condition
											r.p.m	pitch	B.H.P	ton force	Howser / wire		(m)	(ton)	
Bashi Channel	21/12:00	21 33 N 121 57 E			10.9					bc	148.4	20	5800	30	150 220	2	F 11 A 11	45000	unavailable
East Taiwan	22/12:00	25 18 N 124 9 E	259	24:00	10.8					bc	148.4	20	5800	30	150 220	2	F 11 A 11	45000	unavailable
East China Sea	23/12:00	28 40 N 127 38 E	278	24:00	11.6						148.4	20	5800	30	150 220	2	F 11 A 11	45000	unavailable
East Kyushu	24/12:00	31 32 N 131 30 E	269	24:00	11.2														

and towline tension are the items of the emergency towing database. Table 3.2 shows an example of items for the emergency towing database. This list of items is incorporated into the database software in order to retrieve the past towing data to be referred.

3.5 Summary

The flow of the computer system for Optimum Towing Support System (OTSS) was introduced and English version of the instruction manual was produced for the use of the actual towing operation in France. The issues of OTSS were also shown and those should be incorporated in the future. The system will be improved evaluating the results of practical operation of OTSS.

The emergency towing database was also proposed to be utilized for the rescue organizations in foreign countries. It is necessary to use the OTSS system during towing in order to produce this database. The actual data are stored in the computer system after the towing operation and the towing database is automatically produced.

References

1) Hara S., "Research outline on prevention of disabled ships in rough seas (Optimum Towing Support System)", Proceedings of the 74 th Meeting at Internal meeting of Ship Research Institute, 2000.

2) Hara S., "Optimum Towing Support System (part 1: Final status of damaged ship)", Proceedings for 1st Internal meeting of National Maritime Research Institute 2001.

3) Hara S., " Optimum Towing Support System (part 2:)", Proceedings for second Internal meeting of National Maritime Research Institute 2002.

4) Haraguchi T., Nimura T., "Measurement of Wave Drift Force Acting on Tug and Barge at Zero Froude Number", Report of Ship Research Institute, Vol.31, No.3, 1994.

5) Maruo,H., "The Drift of a Body Floating on Waves", Journal of Ship Research, Vol.4, No.3, 1950.

6) Newman,J.N., "The Drift Force and Moment on Ships in Waves", Journal of Ship Research, Vol.11, No.1, 1967.

7) Yuasa H., "Impact on 3D-web and engineering", Journal of Japanese Society of Naval architects, Vol.871, 2003.

8) Ueno M., Nimura, T., Miyazaki H., "On Steady Drifting Motion of Disabled Ships", Journal of Japanese Society of Navalarchitects, Vol.192, 2002.

9) Yukawa K., Hoshino K., Hara S., Yamakawa K., "Hydrodynamic Forces Acting on Capsized With Geometrical Configuration and the Towing Method", Journal of Japanese Society of Naval Architects, Vol.186, pp.145-156, 1999.

10) Yukawa, K., Hoshino K., Hara S., Yamakawa K.,"On the Towing of Wrecked Tanker's Fore Part at Rough Sea" , Journal of Japanese Society of Naval Architects, Vol.191, 2002a.

11) Yukawa, K., Hoshino K., Hara S., Yamakawa K., "An Estimation of Hydrodynamic Forces Acting on a Trimmed Ship Hull" , Journal of Japanese Society of Naval Architects, Vol.192, 2002b.

4. Research on Heavy Oil Monitoring by Lidar

4.1 Introduction

Today, huge amounts of petroleum oil are imported to Japan, and almost all of them are transferred by ship. A tanker accident that has caused an oil spill is a potential crisis leading to severe ocean pollution. It may affect the coastal biosphere and human economic activities seriously. In 1997, the tanker NAKHODKA broke in two parts in the Sea of Japan in foul weather, and more than 6,000kl of heavy fuel oil (class C) was spilled over. In cases like this, immediate response is necessary to guard against oil pollution using oil booms, oil skimmers and oil recovering vessels. In reality, the visual recognition of heavy fuel oil on the ocean was possible only in daytime, and then not easy during foul weather condition[1]. Therefore, to facilitate the response to such oil pollution issues, it is very important to develop a powerful monitor system that is useful for getting precise information about oil spills.

NMRI has developed a new, helicopter-based, fluorescence imaging Lidar. This is an active remote sensing system aimed for real-time monitoring of oil spill position, scale and type. Both high mobility to the accident site and slow scanning around the area are achieved by the helicopter onboard remote-sensing system.
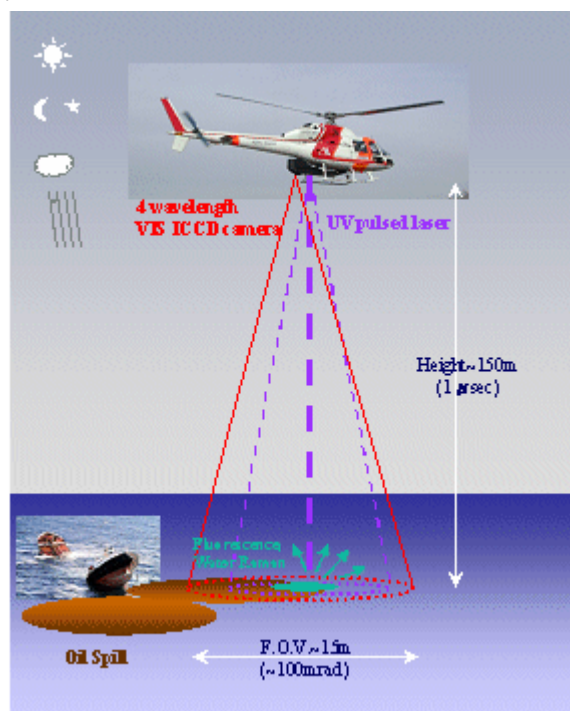
The laser induced fluorescence detection is a reliable visualization method for oil spills by day or night[2]. Additionally, not only heavy, light, or crude oil, but also some kinds of petroleum chemicals can be the target material of the system, which is limpid and hard to identify visually on the ocean. The conceptual diagram of the system is shown in Fig. 4.1.

The performance evaluation test was necessary for the system in similar situation of heavy oil disaster. Japan and France made an agreement for collaborative research on Lidar testing and heavy fuel oil monitoring on the ocean, and the program was implemented.

4.2 Laser-induced oil fluorescence

The petroleum oil emits fluorescence when it is induced by UV laser. The pattern of an oil fluorescence spectrum depends on the wavelength of the induced laser and molecular structure of oil. In general, oil is a mixed liquid of various organic polymer molecules. Therefore, there are many processes of laser excited fluorescent emission, and its wavelength spectrum is broad over a wide range.

In the helicopter-based Lidar system, we have chosen a Nd:YAG pulsed laser with a third-harmonic generator, which is reasonably compact, stable and high power. For checking the emission spectrum of target oil excited by this laser, we emulated the condition of an oil spill detection in the laboratory. As shown in Fig.4.2, target oil was floated on distilled water in a beaker and laser was shot from above the target. At the bottom of the beaker, a piece of unglazed ceramic was put as a laser beam damper.

The emission spectrum was measured for heavy fuel oil, diesel oil, kerosene, distilled water and sea

Fig.4.1 The conceptual diagram of the helicopter-based fluorescence imaging Lidar.
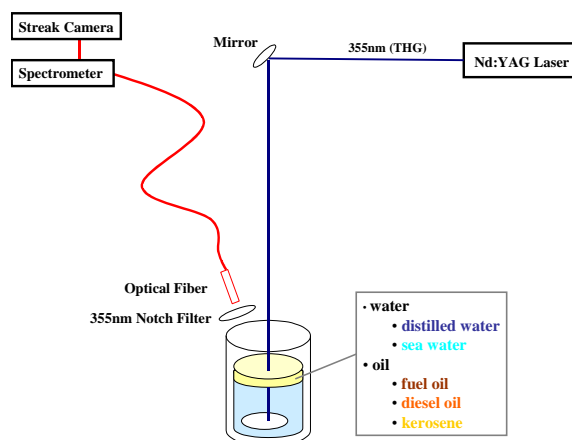

Fig.4.2 The schematic of the time-resolved oil film fluorescence spectroscopy measurement.
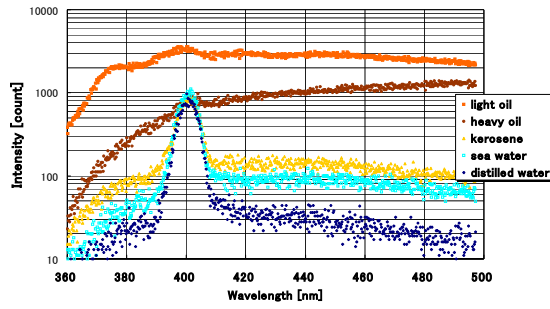
Fig.4.3　The Nd:YAG(THG) laser induced emission spectroscopy from distilled water, sea water, kerosene, heavy oil and diesel oil.

water from off the coast of Kochi, Japan. The emission light from target was collected by the optical fiber with the 355nm optical notch filter. The fiber guided the emission light to the spectroscope CHROMEX 250IS, and then the spectroscopic light is measured by the streak camera HAMAMATSU C5680 for getting time-resolved fluorescence spectroscopy.

As a consequence of measurements, we confirmed that the distilled water and the seawater emission spectrum have a characteristic peak due to water-Raman scattering at wavelength 405nm3). On the other hand, three types of oil have no characteristic peak, but have broad and strong fluorescence spectrum around wavelength 400 to 600nm. The spectrum pattern is unique for each type of oil. The fluorescence spectrum from the target oil is shown in Fig. 4.3.

Additionally, each type of oil has a specific fluorescence period, and the diesel oil has a longest attenuation time, around 30 nano seconds. The emission transition curve from target oil is shown in Fig. 4.4.
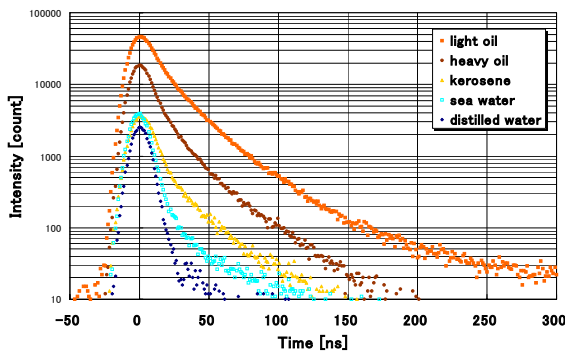In the helicopter-onboard system, we designed to use

Fig.4.4　The UV pulse laser induced emission transition curve from distilled water, sea water, kerosene, heavy oil and light oil. The horizontal axis is normalized at maximum emission timing.

four optical filters to obtain the wavelength information of fluorescence instead of the spectroscope. This design allows the observation of image signal at four specific wavelengths. The four optical filter transmittances for the helicopter-onboard system are shown in Fig. 4.5.
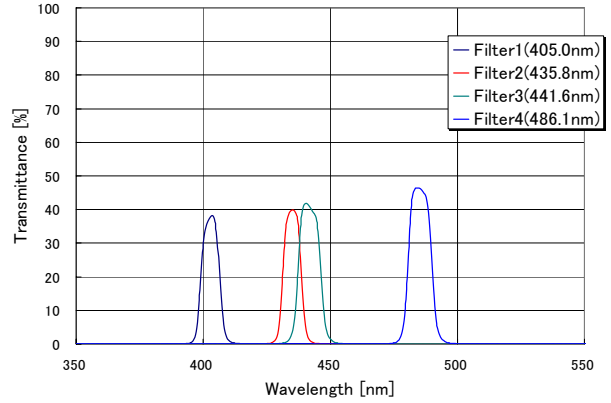

Fig.4.5　The transmittance spectra of four optical narrow band filters used in the Lidar experiment.

4.3 Helicopter-based imaging Lidar system

The NMRI imaging Lidar system mainly consists of three parts; the laser transmitter, the receiver optics, and the gated 2-D photo-sensor.

A frequency-tripled, Q-switched Nd:YAG laser (Quantel BigSkyLaser CFR400) is used as a transmitter. The pulsed laser of wavelength 355nm induces sea surface with an approximately one milli radian beam divergence. The beam intensity is approximately 40mJ with a repetition rate of 4Hz. Eye-safe conditions are satisfied at sea level when the helicopter keeps its altitude at 100m or more.

The photo-detector is a gated image- intensified CCD (ICCD) camera (HAMAMATSU C7972-03). The photo-sensing focal plane of the image intensifier is split into four parts, and each part is used as a photo-sensor for four independent optical systems. The four optical systems consist of four condenser lenses and optical filters of 50mm diameter, and their viewing angle is approximately 100 milliradian for each. Each field of view is overlapped at infinity. This optics is designed for recording four views of same image but of different wavelengths simultaneously. Optical filters installed in front of the condenser lenses are narrow band pass filters with peak wavelengths of 405.0, 435.8,

17

441.6, 486.1nm respectively, and the full-width half-maximum (FWHM) of narrow band is 10nm. The pixel size of the CCD camera is 1024 x 1024, and one image with one wavelength corresponds to 512 x 512 with 12bits (4095 levels) intensity resolution in each pixel. By using optical filters and a fixed ICCD camera, instead of a spectroscope and a scanning optics, the resulting system is light and robust and utilizes simple real-time monitoring.

To obtain a fluorescence Lidar signal with higher signal-to-noise ratio, the ICCD camera is only exposed for several hundred nano seconds, including the moment that the laser scattered light at sea surface reaches the ICCD camera. This method drastically reduces the noise due to scattered sunlight near the sea surface without reducing the fluorescence Lidar signal. For this gating method, it is necessary to preset the distance from the Lidar system to the sea surface along with laser track, and control the gate open and close timing of the image intensifier. Since the laser track constantly changes with the position and attitude of the helicopter, the previous duration between laser Q-switch and detection of scattered light at the sea surface are used to estimate the preset distance for the next Lidar measurement.

The position and attitude data are measured and transferred to PC and stored in it by the repetition of 5

Hz. Additionally, the GPS clock data are recorded at every Q-switch timing. Since laser shooting repetition is 4Hz, the preset distance is also updated at 4Hz using a special circuit. The data of the observed 2-D image are transferred from the ICCD camera to the PC at every shot through IEEE1394, and stored in it.

Meanwhile, the position and attitude of the helicopter are also recorded. To measure the position, GPS system AEROANTENNA TECHNOLOGY AT575-62 and ASHTECH G12 SENSOR are installed. In good conditions when receiving signals from several GPS satellites, the accuracy of position (latitude, longitude, altitude) measurement is approximately 1m.

To measure the attitude, a fiber optic gyro (FOG) attitude measurement system JAE JCS7401A is installed. This is a system consisting of a gyro and an accelerometer, with an accuracy of attitude (roll, pitch, yaw) measurement of better than 0.2 degrees.

The block diagram of the NMRI helicopter based fluorescence imaging Lidar is shown in Fig. 4.6, and its specifications are shown in Table 4.1. The photograghs of the Lidar system are shown in Fig. 4.7.

All equipments are packed in three racks; a belly rack which is installed under the helicopter body, a cabin rack which is installed in the helicopter cabin in front of Lidar operators, and a power rack which is installed in the space beside the helicopter electric generator and supplies AC 100V to the Lidar system. The weight of each rack including all equipments is 108.2kg, 56.9kg, and 16.4kg respectively. In this test

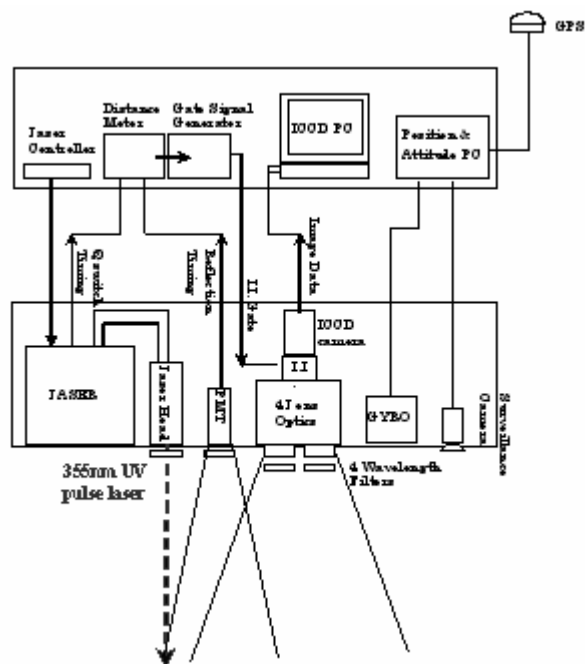Fig.4.6   The block diagram of the NMRI helicopter based fluorescence imaging Lidar.

Table 4.1 The specifications of NMRI helicopter-based fluorescence imaging Lidar.

| Laser	Type	Nd:YAG(THG)
	Wavelength	355nm
	Energy	40mWpulse
	Repetition	4Hz (Max 10Hz)
	Beam Divergence	1mrad
Optical filter	Peak wavelength	405, 436, 442, 486nm
	FWHM	10nm
ICCD camera (Image Intensifier + CCD camera)	II. Gain	<7 *10⁴
	CCD camera Pixel Size	1024 *1024 (512*512 /filter)
	Digitizing	12bit
	F.O.V.	100mrad
	Recording Repetition	4Hz
Distance Meter	Distance Resolution	0.75m
GPS	Position Resolution	0.9m horizontal 1.6m vertical
Attitude Measurement Equipment	Attitude Resolution	0.2deg
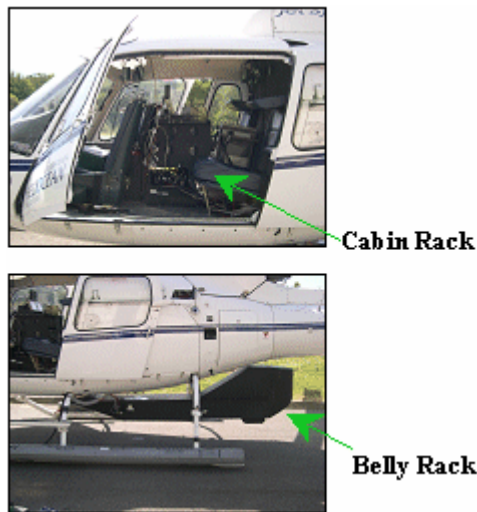
Fig.4.7   The photographs of the NMRI helicopter based fluorescence imaging Lidar.

observation, these racks were mounted on the AEROSPACIAL AS350B, a typical civilian helicopter.

4.4 Test observation of oil spill

The international experiment of oil spill monitoring and recovery, "DEPOL04", was held from 25/May/2004 to 27/May/2004 off the coast of France. This experiment was organized by CEPPOL (Commission d'Etudes Pratiques de lutte AntiPOLution), French Customs, and CEDRE (Centre de Documentation de Recherche et d'experimentation sur les pollutions accidentelles des Eaux). On 26/May, the 9m^3 of heavy fuel oil was released into the sea, and then its behavior was monitored. Finally it was recovered by oil recovery vessels. The view of an oil spill from the helicopter is shown in Fig. 4.8. The weather was clear with weak winds and waves. The released oil had been spread in a hundred meter diameter roughly.

The NMRI helicopter onboard Lidar observation was operated from 7:30 to 8:00 a.m. local time. Since it was in the morning, the background light caused by sunlight scattering at the sea surface was low from a vertical position. The helicopter altitude and velocity are shown in Fig. 4.9.

The observation of the oil spill was conducted using two methods. One way was the Lidar observation by shooting UV pulsed laser vertically downward and receiving the laser-excited fluorescent light from the oil spill within 400ns by the four wavelengths ICCD camera. The other way utilized passive observation by

Fig.4.8   The view of an oil spill from the helicopter during "DEPOL04".
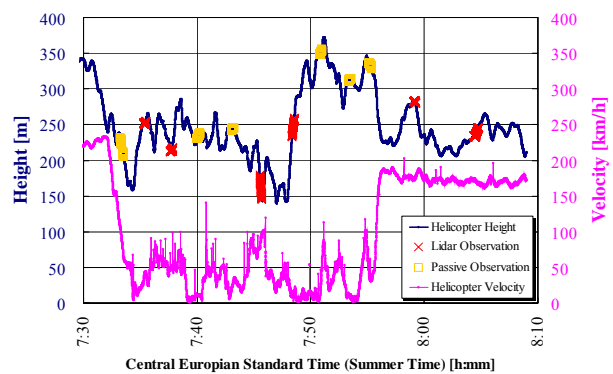
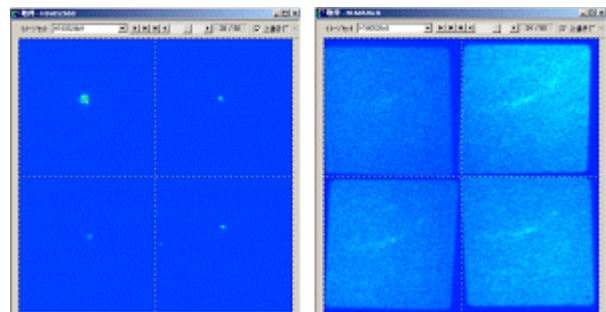Fig.4.9   The helicopter height and velocity during the observation.

Fig.4.10 The ICCD sample images.
Left: Lidar observation (gate 400ns, height 157m).
Right: passive observation (gate 0.5ms, height 332m).
The center wavelengths of optical filters are 405, 436, 442 and 486nm respectively counter clockwise from up-left.

receiving the scattered sunlight from the oil spill within a 0.5ms gate width with no timing relation between laser shot and the ICCD camera gate. In Fig. 4.9, the cross plots show the Lidar observation position, and the square plots show the passive observation position. The sample of ICCD images obtained by Lidar observation is shown in Fig. 4.10. The intense spot from water-Raman scattering of UV laser can be seen at the

405nm ICCD image. The sample of ICCD images obtained by passive observation is also shown in Fig. 4.10. In the passive observation, the ICCD camera receives scattered sunlight at the sea surface and the images show the shape of spread oil. This result implies that in sunny daytime, passive sensing is also effective in detection of oil spills by the ICCD camera.

4.5 Lidar data analysis

The Lidar data observed on the oil spill area are analyzed by the following procedures. At first, the signal region, 63 by 63 pixels square area, is fixed on each ICCD image with centering of maximum light intensity pixel. In the case of a helicopter altitude 150m, this signal region corresponds to a 1.9m by 1.9m square area on the sea surface. The background area is set on both sides of the signal area at a four times larger size. The background value is calculated by the sum of the light intensity level of all the background area and then divided by four to normalize the area size. The signal value $S(\lambda)$ is calculated by the sum of the light intensity level for all the signal area and then subtracted the background value.

$$S(\lambda) = \sum_{x}^{63}\sum_{y}^{63} I_{sig}(\lambda, x, y) - \frac{\sum_{n}^{4}\sum_{x}^{63}\sum_{y}^{63} I_{b.g.}(\lambda, n, x, y)}{4} \quad (4\text{-}1)$$

Here, λ is the numbering of the optical filter, x is the horizontal pixel of remarked area, y is the vertical pixel, $I_{sig}(\lambda, x, y)$ is the light intensity level at one pixel in the signal area, n is the numbering of the noise area, $I_{b.g.}(\lambda, n, x, y)$ is the light intensity level at one pixel in the noise area.

The Lidar target material is estimated by the signal values of four wavelengths. Fig. 4.11 shows the signal and background area in a 2-D image of each wavelength.

The signal value of wavelength 405nm is used as a criterion, since the water-Raman signal is dominant at this wavelength when the clear sea water is irradiated by a 355nm laser. The ratios of 436, 442, 486nm to 405nm are used to distinguish the target material. This method emphasizes the oil fluorescence signal from the water-Raman signal emitted in seawater.

The obtained Lidar observation data on the oil

spill area are 4 sets with different conditions and 50 shots in each set. The event selection from all 200 shots takes place under the following conditions; the average signal values for each set and each wavelength are calculated. The events are chosen with the condition that all four signal values are more than 10% of the average signal values of the corresponding set. 111 shots remained out of 200 shots using this event selection. Fig. 4.12 shows the three ratio patterns in each shot. The vertical axis has an offset value of 0.2 times of the event number for easy visibility. In this graph, almost all shots show the typical sea water pattern, but several shots show quite different patterns from the typical sea water. These unusual patterns have a strong possibility of oil spill detection.
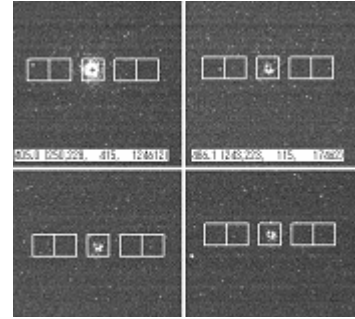

Fig.4.11 Signal areas and background areas for calculation of signal value from Lidar observation images.
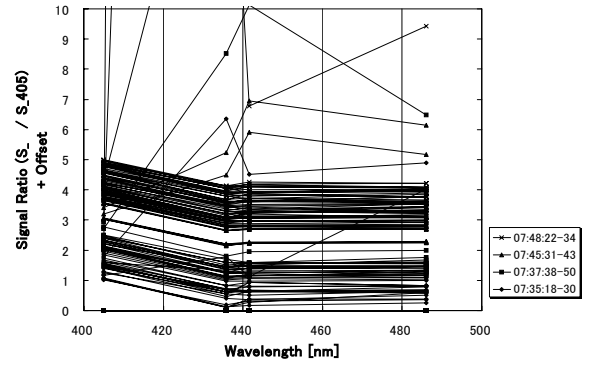

Fig.4.12 The three wavelength lidar signal ratios for each shot.

4.6 Conclusions and Further Developments

We have developed a helicopter-based fluorescence imaging Lidar system for real-time monitoring of oil disasters, and the test observation has been operated off the shore of Brest in France as a collaboration of DEPOL04. During the operation, four
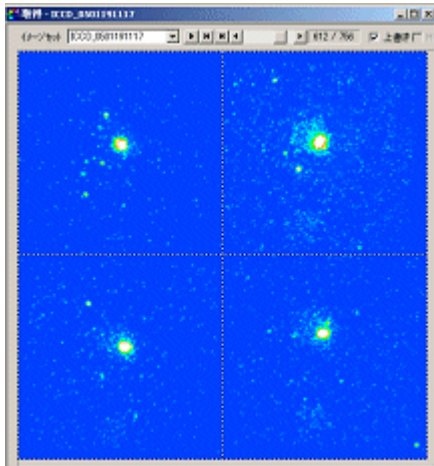
Fig.4.13 The ICCD sample image of Lidar observation of diesel oil (gate 200ns, height 121m). The center wavelengths of optical filters are 405, 436, 442 and 486nm respectively counter clockwise from up-left.

wavelength 2-D images of Lidar signals were obtained with a target of oil spill and seawater.

Through the checking of signal value from four wavelength 2-D images of Lidar observation data, and comparing the signal ratio to water-Raman channel, we found the typical seawater patterns, and some unusual pattern events. These events have a possibility of sensing oil spill which are formed as a thin film of heavy fuel oil on the sea surface. The oil spill shape on the ocean has been observed by passive observation under daylight, and it implies a possibility of high-speed, wide-view oil spill monitoring using an ICCD camera in sunny daytime.

We could not have a strong evidence of heavy fuel oil detection on the sea surface by Lidar observation. The possible reason is that we missed recording "hit" events that show strong fluorescence from oil. The observation time was short and it was difficult to record data when the helicopter flew on the oil spill. Another possible reason is that high viscosity heavy fuel oil formed uneven thickness oil spill, and the thin oil film area would be difficult to measure by Lidar.

After DEPOL04, we found out several points to be upgraded, and improved the Lidar system for continuous data recording, laser beam divergence control, and higher repetition observation. Then, another helicopter experiment has been held in Japan with targets of diesel oil and kerosene, and succeeded in detecting them clearly by the Lidar observation. The example of the Lidar observations of diesel oil is shown in Fig. 4.13.

References
1) MINISTRY OF LAND, INFRASTRUCTURE AND TRANSPORT, (2004), Recent main oil spill accidents by tankers, White Paper on Efforts against Ocean Pollution - response to the massive oil spill -, pp.15 (written in Japanese)
2) VISSER, H., (1979), Teledetection of the thickness of oil films on polluted water based on the oil fluorescence properties, Applied Optics, Vol.18, No.11, pp.1746-1749.
3) BARTLETT J. S., VOSS K. J., SATHYENDRANATH S. and VODACEK A. (1998), Raman Scattering by Pure Water and Seawater, Applied Optics, Vol.37, No.15, pp.3324-3332.

5. Summary

There are mainly three research themes in this cooperative project between Cedre and NMRI. Those are the research on oil discharge in Ice covered area, research on Optimum Towing Support System and research on heavy fuel oil monitoring by LIDAR.

The purpose of this research is mainly divided into three

As for the oil problem in ice, the behavior of oil spilled under an ice cover was studied. The study was made for two different points related to the oil in ice. One is the spreading behavior of oil under an ice cover and the other is the deformation and drifting motion of an oil slick due to current under the ice. Experimental and numerical studies were made for the both problems. The spreading behavior of oil under an ice cover is very much affected by the underside configuration of the ice. A simple model to account for the effects of the size of the underside roughness of the ice cover was given. The model well explained the results of the experiment and numerical simulation on the spreading or the oil under an ice cover. The deformation and drifting motion of an oil slick under a level ice sheet was also studied experimentally. The experiment showed the thickening of the front edge of the oil spill under the effect of current. The experimental results were taken in the numerical model to simulate the deformation and drifting or an oil slick due to current. The calculated results qualitatively agreed with the experimental ones.

As for the OTSS, the English version was produced and English system manual was also maintained. However, the operational evaluation has not been done due to lack of data gathered. The format of making the emergency towing database has only been completed. The performance data of the expected tugboat is needed in order to evaluate the OTSS system operationally. Those data should be incorporated into the OTSS system. The new 3 year research project started and this research topic will be researched continuously.

As for the monitoring system of discharged heavy fuel oil, a helicopter-based fluorescence imaging LIDAR system for real-time monitoring of oil disasters has been developed. The test observation has also been operated off the French shore as a collaboration of DEPOL04. During the operation, four wavelength 2-D images of LIDAR signals were obtained with a target of oil spill and seawater. The LIDAR system for continuous observation and the adjustment system of laser beam divergence and 8Hz high repetition observation have been improved after DEPOL04. NMRI already participated in the Depol'05 October in 2005 and would like to participate in the both Depol'06 and Depol'07.

Acknowledgement

Description of OTSS manual

The flow of OTSS is elaborated using the monitor display in the computer.

(1) Display for starting (Fig.A1)

When OTSS is executed, this display appears. When you start the calculation, push **'start'** button. When this button is pushed, the starting display will disappear and the next display for **'input data selection'** will appear instead.

When you do not calculate, push **'quit'** button. When this button is pushed, the starting display will disappear and the system will stop.

Date of execution

Push this button when to start calculation

Push this button when to quit
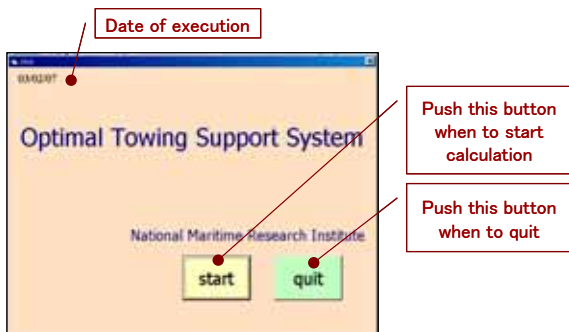
Fig.A1   Display for starting

(2) Display for input data selection (Fig.A2)

You can select the input method for data from 3 kinds of button such as **'New'**, **'Past results'** and

Check this button for new input data

Check this button when to refer to the default results for designated sea conditions

After checking one of the three choices, push this 'input' button.

When the calculation is not done anymore, push this 'quit' button

Check this button when to refer to the past results
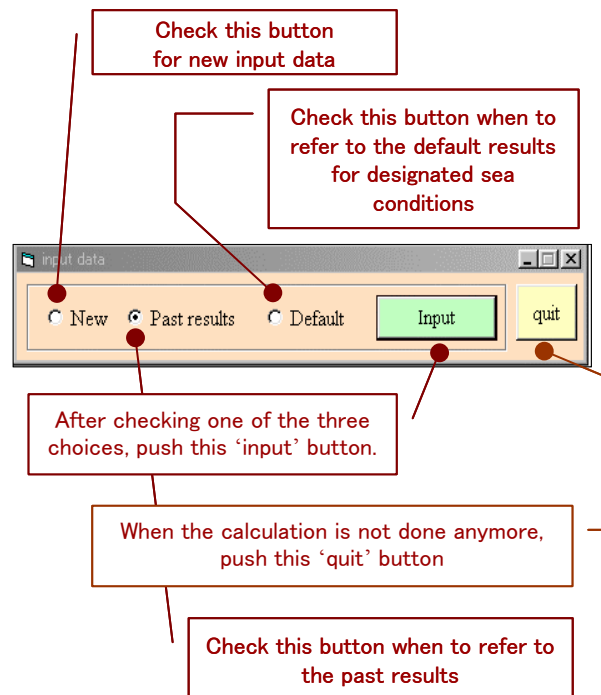
Fig.A2   Display for input data selection

'Default'.

When you calculate for new input condition, check **' New'** and push **'Input'** button. Then Main display will appear.

When you refer to the past calculated results, check **'Past results'** and push **'Input'** data. Then the display for the selection of the past results will appear.

The path name of folder in which data are stored is shown

This is selection box for drive. Default drive is C.

This is selection box for folder. The default is c:¥vbotssNETEnglish2¥save

Push this button after selecting the folder.

Push 'File Load' button and confirm data in the note. Then push this button

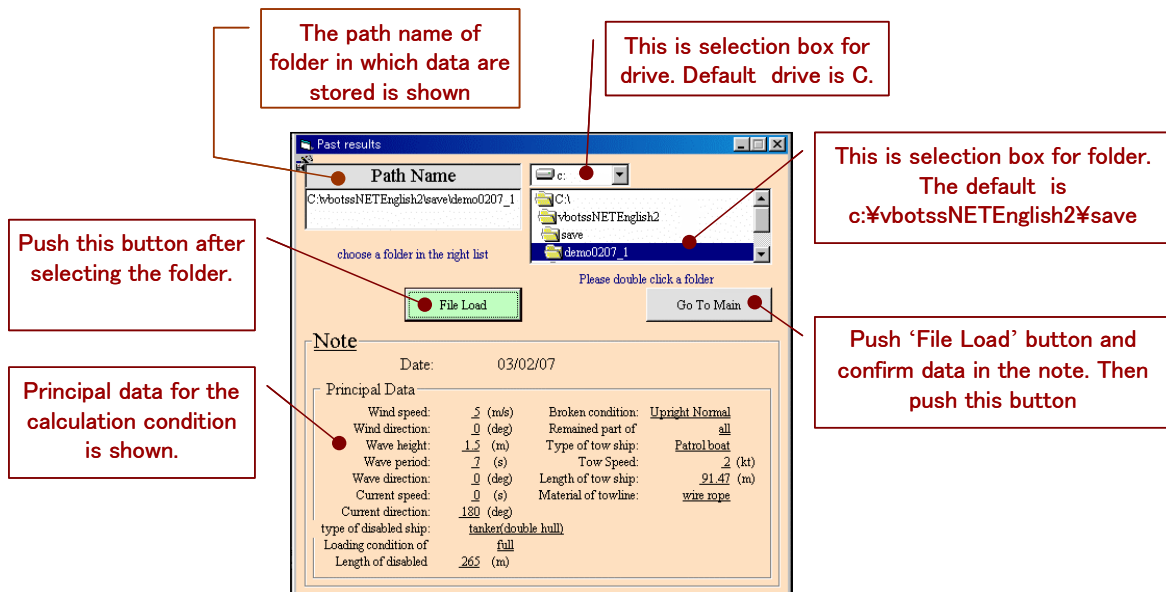Principal data for the calculation condition is shown.

Fig.A3 Display of selection for past calculated results

When you refer to the default results calculated on designated sea condition, check **'Default'** and push **'Input'** button. Then the display for default calculated results will appear. When you do not calculate any more, push **'quit'** button. Then the display for the input data selection will disappear and the system will stop.

(3) <u>Display of selection for past calculated results</u> (Fig.A3, Fig.A4)

Input procedure
1. Select the drive in the drive box. C drive is recommended in this system.
2. Double click the folder in which data is stored in the folder selection box. Keep the picture of the file open (see below figure). Do not open the folders such as **'files'** and **'results'** under the data saved folder.
3. Push **'File Load'** button. Then the date of execution and principal calculation conditions are shown.
4. Push **'Go to Main'** button. Then the display of ' Display of selection for past calculated results' will disappear and **'Main display'** will appear.

(4) <u>Display for input of default calculated results</u> (Fig.A5)

Input procedure
1. Select one out of weather condition selection box. 7 weather conditions are shown as below.
   * wind speed 5 m/s、 wave height 0.5 m、 wave period　5.0 sec
   * wind speed 7 m/s、 wave height 1.0 m、 wave period 5.0 sec
   * wind speed 7 m/s、 wave height 1.0 m、 wave period 7.0 sec
   * wind speed 10 m/s、 wave height1.5 m、 wave period7.0 sec
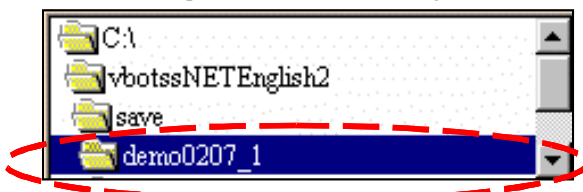   * wind speed 10 m/s、 wave height 1.5 m、 wave
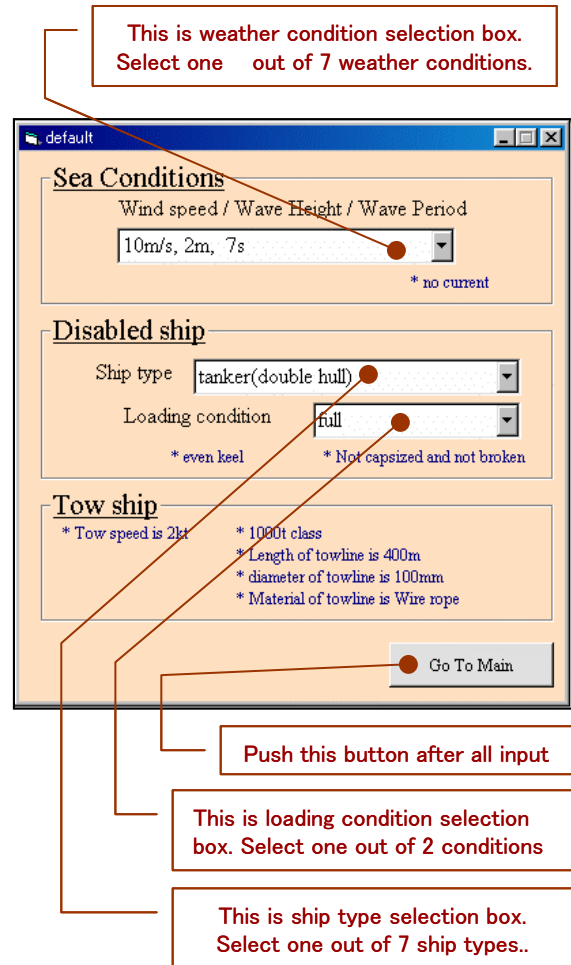

Fig.A4　Enlarged figure of selection box

Fig.A5　Display for input of default calculated results

   period 9.0 sec
   * wind speed 12 m/s、 wave height 2.0 m、 wave period 9.0 sec
   * wind speed 15 m/s、 wave height 3.0 m、 wave period 10.0 sec

2. Select one out of ship types selection box;. 7 ship types are shown as below.
   * tanker (double hull)
   * tanker (single hull)
   * cargo
   * container
   * fishing boat
   * PCC
   * barge

3. Select one out of loading condition selection box. 2 loading conditions are shown as below.
   * full load　　* 　ballast

24

4. Push **'Go to Main'** button. The display for input default calculated results will disappear and main display will appear.

(5) <u>Main display </u>(Fig.A6)

＊ Corresponding table

This table shows the input data needed to calculate the required items.

Example) Input data for **'Sea condition'**, **'Size and Shiptype Loading'**, **'Broken condition etc.'**, **'Tow Ship and Towline'** and **'Maneuver'** have to be input to calculate maneuvering simulation. After calculating hydrodynamic forces, maneuvering simulation can be done.

＊ Input items

First data for **'Sea condition'** or **'Size, Shiptype and Loading Condition'** have to be input. Then **'Broken condition etc.'** or **'Tow ship and Towline'** have to be input. When the needed data are input, the check mark **"✓"** appears on the right side of the each button. When check mark **"✓"** does not appear, you cannot proceed to the next step.

・When you push the button **'Sea condition'** , **'Display for sea condition'** is shown,
・When you push the button **'Size, Shiptype and Loading'**, **'Display for input of principal**

dimensions of disabled ships' is shown.
・ When you push the button **'Broken condition of disabled ships. Calculation of center of gravity and damage stability'**, **'Display of input for broken condition of disabled ships'** will appear.
・ When you push the button **'Specification of tow ship and towline'**, **'Display of input for tow ship and towline'** will appear.

＊ Calculation

Calculation of hydrodynamic forces should necessarily be done. After this calculation drift motion simulation and maneuvering simulation can done.

・ When you push the button **'Hydrodynamic Force'**, the display of **'Calculation of hydrodynamic force & motion'** will appear.
・ When you push the button **'Steady drift'**, the display of **'Steady drift calculation'** will appear.
・ When you push the button **'Maneuver'**, the display of 'Maneuver simulation' will appear.

＊ Others
・When you close the display of **'Main'**, push the button **'Close'** .

(6) <u>Display of sea condition </u>(Fig.A7)
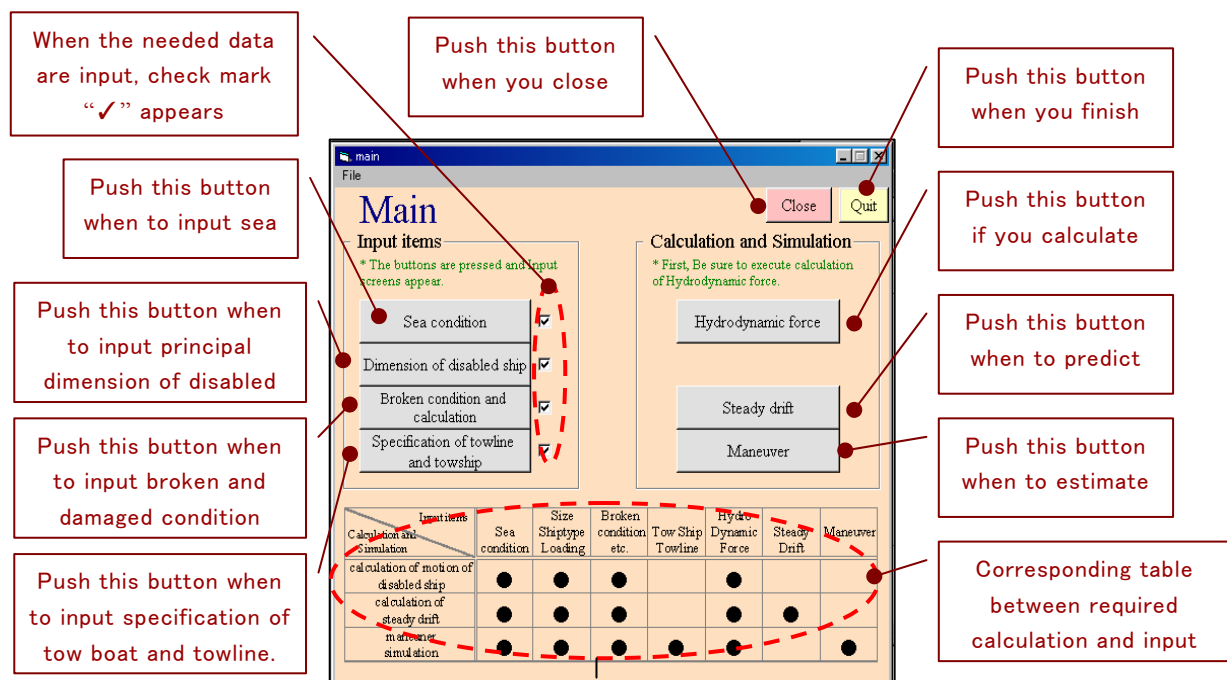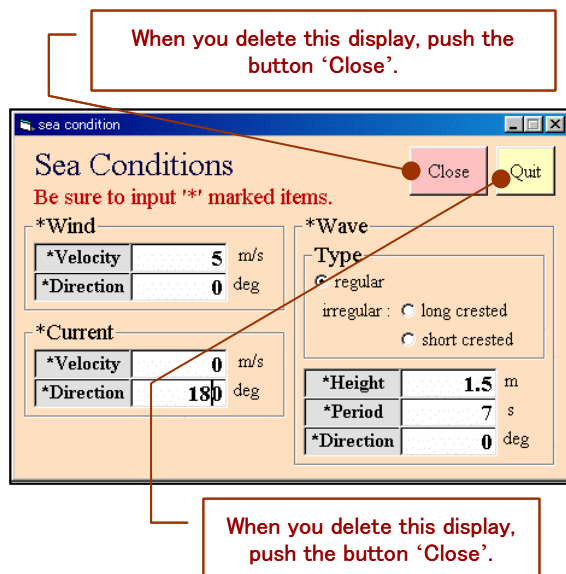

Fig.A6　Main display

25

Fig.A7   Display of sea condition

・When you finish the system, push the button **'Quit'**.

Data for sea condition should be input in this display.
    The digital value should be input in half size.

∗   Wind
    ・The unit of the wind speed is m/s.
    ・The unit of the wind direction is degree. The wind directions coming from north and south are defined as 0deg and 90deg respectively

∗   Current
    ・The unit of the current speed is m/s.
    ・The unit of the current direction is degree. The current   direction coming from south to north is defined as 0deg. The current direction coming from west to east is defined as 90deg.

∗   Wave
    ・The regular wave is automatically selected in the kinds of coming waves. Irregular waves such as long and short crested wave are not included.
    ・The unit of the wave height is m.
    ・The unit of the wave period is sec.
    ・The unit of the wave direction is degree. The wave direction coming from south is defined as 0deg. The wave direction coming from east is defined as 90deg.

∗   Others
    When you delete this display, be sure to push the button **'Close'**.

(7) Display of 'Principal dimension of disabled ship' (Fig.A8)

    Input principal dimensions of disabled ship in this display.
    The digital value should be input in half size.

∗   Ship type selection box
    Select one out of 7 kinds of ship types. 7 ship types are as follows.
        ・Tanker(double hull)
        ・Taker(single hull)
        ・Cargo
        ・Container
        ・Fishing boat
        ・PCC
        ・Barge

∗   Loading condition selection box
    Select one out of 2 loading conditions. 2 loading conditions are as follows.
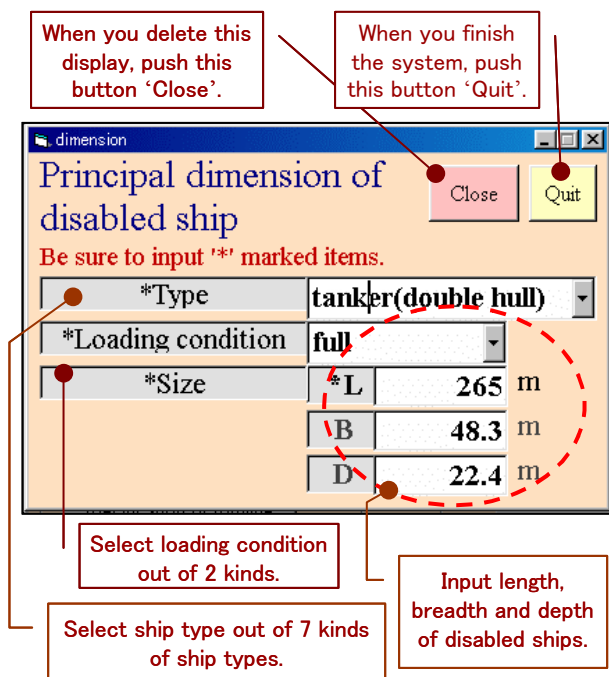   ・   Full
        ・   Ballast

Fig.A8   Display of **'Principal dimension of disabled ship'**

26

∗ Principal dimension

Input the length, breadth and depth of disabled ship. If the breadth or depth is unknown, you have only to input length data. The breadth and depth are automatically calculated from stored mother ship type.

The dimension of mother ships is as follows.
・Tanker(double hull)　→　L = 320m　B = 58m　D = 28.8m
・Tanker(single hull)　→　L = 265m　B = 48.3m　D = 22.4m
・Cargo　　　　　　　→　L = 156m　B = 26.6m　D = 14.1m
・Container　　　　　→　L = 200m　B = 32.0m　D = 16.5m
・Fishing boat　　　　→　L = 53m　B = 9.4m　D = 4.01m
・PCC　　　　　　　　→　L = 180m　B = 32m　D = 14m
・Barge　　　　　　　→　L = 70m　B = 20m　D = 4.01m

∗ Other

When you delete this display, be sure to push the button **'Close'**.

(8) Display of **'Broken condition of disabled ship'**
(Fig.A9)

Input the broken condition of disabled ship in this display.

The digital value should be input in half size.

∗ Broken condition selection box

Select one out of 4 kinds of broken conditions. 4 kinds of conditions are as follows.
・Upright Normal　→　Not broken and upright
・Upright Broken　→　Broken and upright
・Capsized Normal　→　Not broken and capsized
・Capsized Broken　→　Broken and capsized

∗ LC

When you select **'Upright Broken'** or **'Capsized Broken'** in the selection box, input the distance from A.P.(After Perpendicular). This length should not be larger than the length of disabled ship. When you select **'Upright Normal'** or **'Capsized Normal'** in the selection box, you cannot input the value in this box.

∗ Remained part of disabled ship

When you select **'Upright Normal'** or **'Capsized Normal'**, **'all'** is automatically selected. When you select **'Upright Broken'** or **'Capsized Broken'**, select **'fore'** or **'aft'**.

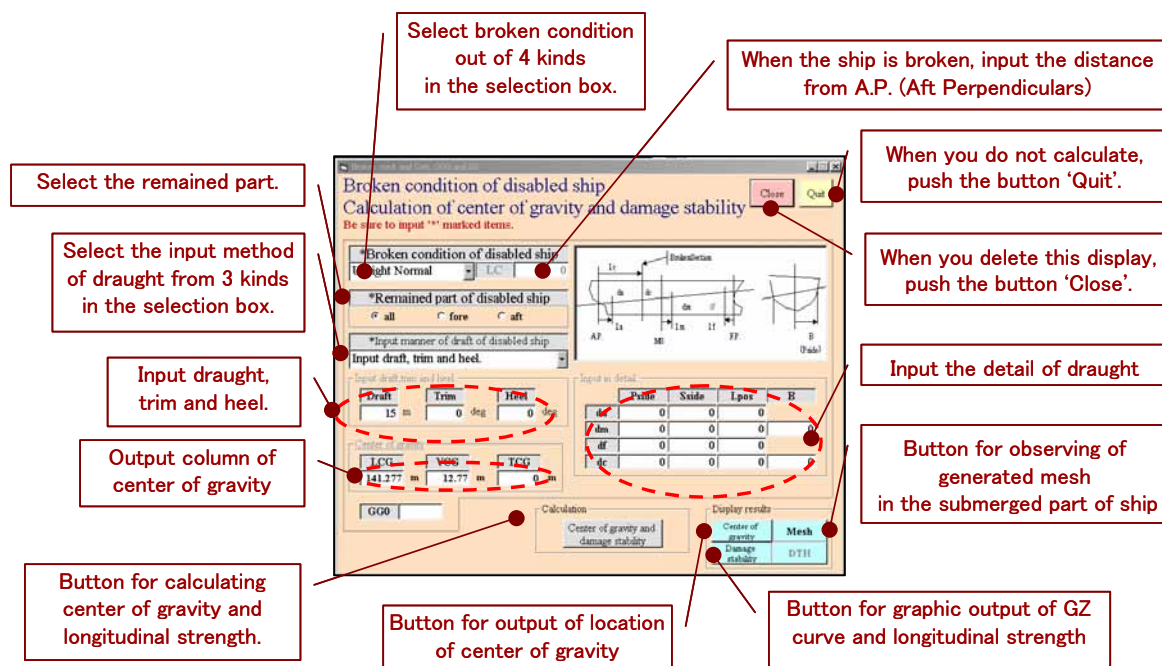∗ Input method of draught of disabled ship

Fig.A9　Display of 'Broken condition of disabled ship'

27

Select one out of 3 kinds of input methods. 3 methods are as follows.

・Input the detail draught at various locations

・Data for **'Draft'**、**'Trim'** and **'Heel'** are only input.

・Input of center of gravity

The input of **'Draft'**, **'Trim'** and **'Heel'** is recommended in this system.

＊ Input of draft, trim and heel

・The assumed mid-draught on normal condition even though the ship is broken should be input. The unit is m.
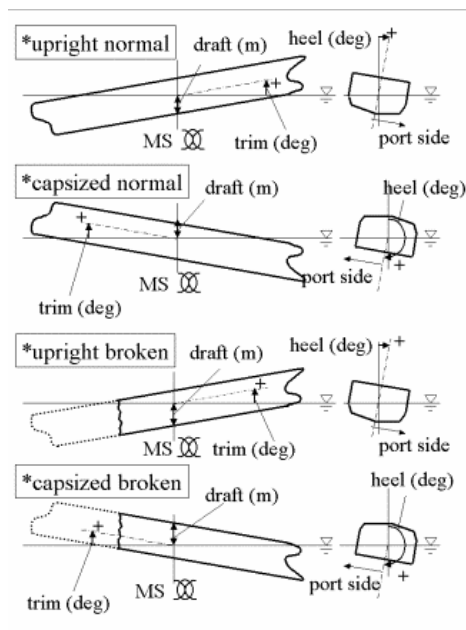
・As for the trim, trim by the stern on upright

Fig.A10　Shape of disabled ship
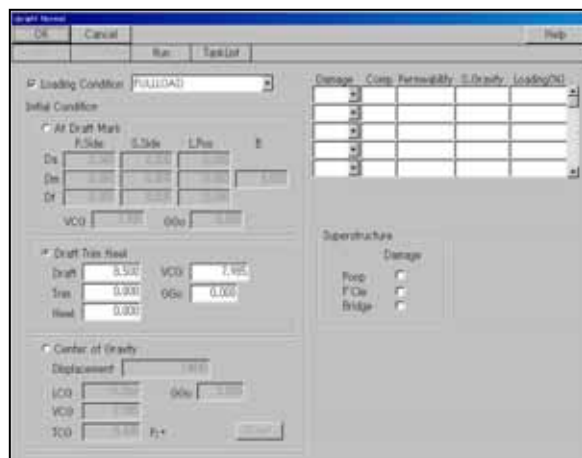
Fig.A11　Display for button of 'Center of gravity and damage stability'

condition is defined as plus sign. On the other hand, trim by the bow on capsized condition is defined as plus sign. The unit is degree (see Fig.A10).

・As for heel, heel where the port is submerged is defined as plus sign (see Fig.A10 on the right side). The unit is degree.

＊ Button of **'Center of gravity and damage stability'** (Fig.A9)

When you push this button, the computer program for the calculation of center of gravity, GZ curve, longitudinal strength is executed. Then the display (Fig.A11) will appear.

When this display appears, push the button **'Run'** and **'OK'** continuously. Then this display will disappear.

[NB]

The error message often comes out on certain condition after pushing the button **'Run'**. In this case you cannot obtain the location of center of gravity, GZ curve, longitudinal strength curve. Further, calculation of hydrodynamic force and drift motion simulation and maneuvering simulation cannot be done. You have to set the new condition again.

＊ **'Center of gravity'** button

The center of gravity such as LCG, VCG and TCG is calculated as an output. If you executed the calculation, you have to push this button.

＊ **'Damage stability'** button　(Fig.A12,Fig.A13)

This button is for the display of GZ curve and longitudinal strength curve. When you push this button, 2 kinds of graphs are shown as Fig.A13. The error message will sometimes come out and graphs will not appear on certain condition.

＊ **'Mesh'** button

This button is for observing the submerged form of ship. When you push this button, the system will execute on the display Fig.A12. When you observe the form, click File(F) and Open(O) in order. Then select **'Wtrmesh.txt'** from the file list and open it.
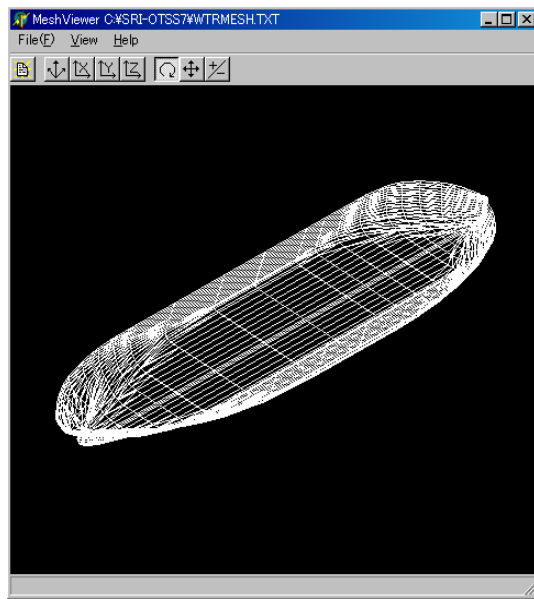
＊ Others
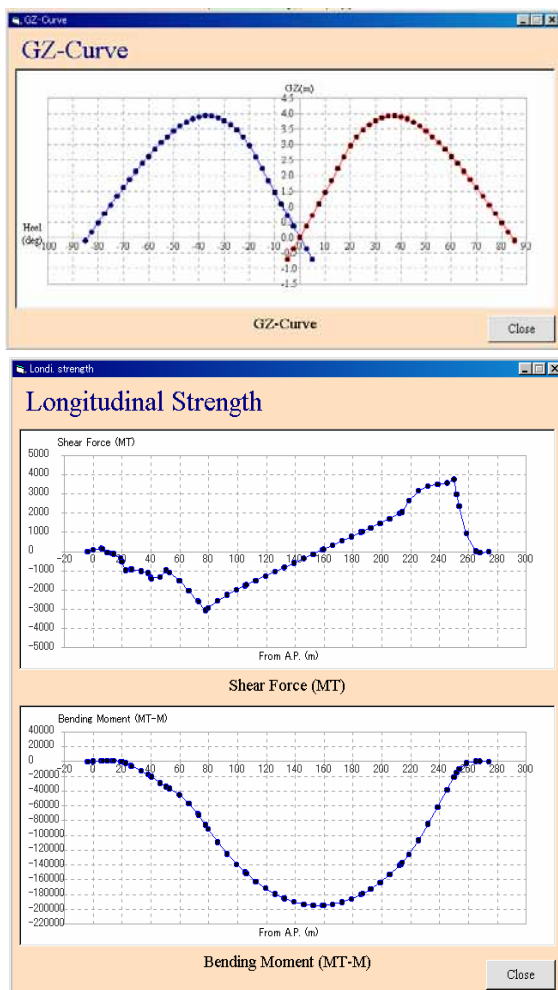
Fig.A12   The submerged form of ship.

Fig.A13   GZ curve and longitudinal
strength curve.

When you delete the display **'Broken condition of disabled ship'**, be sure to push the button **'Close'**.

(9) Display of **'Specification of towship and towline'** (Fig.A14)

Input the specification of towline and towship in this display. The digital value should be input in

Fig.A14   Display of 'Specification of
towship and towline'

29

half size.

∗ Selection box for the towline to be used

Select one out of 2 items such as **'existent'** and **'optimum'**. In this system **'existent'** is recommended.

∗ Kinds of towship

∗ Material of towline

Select the material of towline out of 3 kinds. 3 kinds of material are as follows.
・Dyneema ・Polyethylene ・Wire rope

∗ Tow speed

Input tow speed in 3 columns as below.

Example) from [1] kt to [5] kt at every [1] kt

This example shows 5 patterns such as 1,2,3,4 and 5kt. The number of patterns should be less than 10. Therefore, if you input from [1] kt to [15] kt at every [1] kt, this condition will be rejected because the number of pattern is 15.

If you would like to keep the pattern only one, input from [1] kt to [1] kt at every [0] kt.

∗ tow direction

The tow direction is defined as 0 degree when to go to north and 90 degree when to go to east.

Input the tow direction in 3 columns like below.

Example) from [-60] degree to [60] degree at every [10] degree

The number of patterns to be calculated is 13 in this example. The number of patterns should be less than 73. Therefore、the number of patterns from [-90] degree to [90] degree at every [1] degree becomes 181 and the calculation is rejected.

If you would like to keep only one pattern, input the pattern [10] degree to [10] degree at every [0] degree.

(10) Display for hydrodynamic force calculation (Fig.A15)

When you select **'New'** on the display of input data selection, you have to push the button of **'Force'**, **'Motion'** and **'Animation'** in order.

When you select **'Past results'** or **'Default'** on the display of input data selection, you have only to push the button of **'Animation'** .

∗ **'Force'** button

When you push this button, the computer program for calculating the hydrodynamic force acting on disabled ships is executed. The display on command prompt will come out. You are not allowed to push **'Motion'** button until this display disappears.

∗ **'Motion'** button

Button for executing the calculation of ship motion

Button for executing the calculation of hydrodynamic force

When you do not calculate, push the button 'Quit'.

When you delete this display, push this button 'Close'.
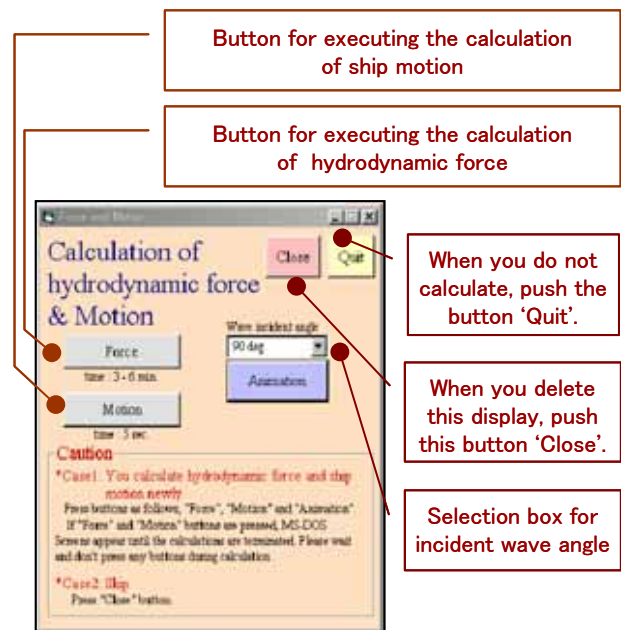
Selection box for incident wave angle

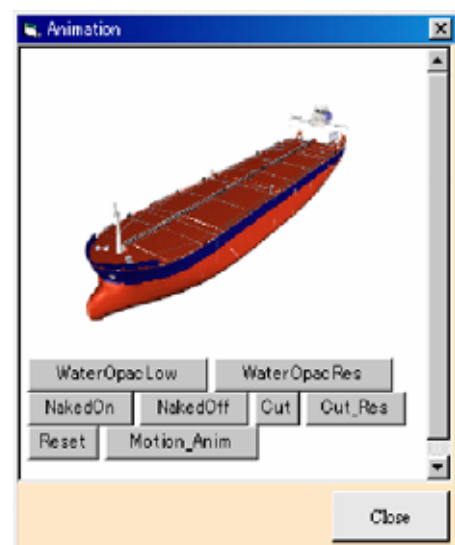Fig.A15 Display for hydrodynamic force calculation

Fig.A16 Display for animation of ship

When you push this button, the computer program for calculating the motion of disabled ships in waves is executed. The display on command prompt will come out. You are not allowed to push **'Animation'** button until this display disappears. (Fig.A16)

∗　**'Animation'** button

This button is for seeing the results of **'Motion'**.

First you select the incident wave angle and push this button. Then the display on the right side will come out.

When you push **'Motion_Anim'** button, the ship on the screen will move for a minute.

The function of other buttons are as follows.

・　**'Water Opac Low**　: The water surface will disappear.

・ **'WaterOpacRes'** : The deleted water surface will appear.

・ **'NakedOn'** : The hull plate will disappear.

・ **'NakedOff'** : The deleted hull plate will appear.

・ **'Cut'** : When the ship is broken, the ship is cut.

・ **'Cut_Res'** : The cut ship will be recovered.

・ **'Reset'** : Keep the ship status even keel condition.

(11) Display for Steady drift calculation (Fig.A17)

When you select **'New'** on the display of **'input data selection'**, you have to push the button of **'Calculation'**, **'Results'** in order.

When you select **'Past results'**, or **'Default'** on the display of **'input data selection'**, you have only to push the button of **'Results'** instead of pushing **'Calculation'**.

∗　**'Calculation'** button

When you push this button, the computer program for calculating the steady drift motion of disabled ships in waves is executed. The display on command prompt will come out. You are not allowed to push **'Results'** button until this display disappears.
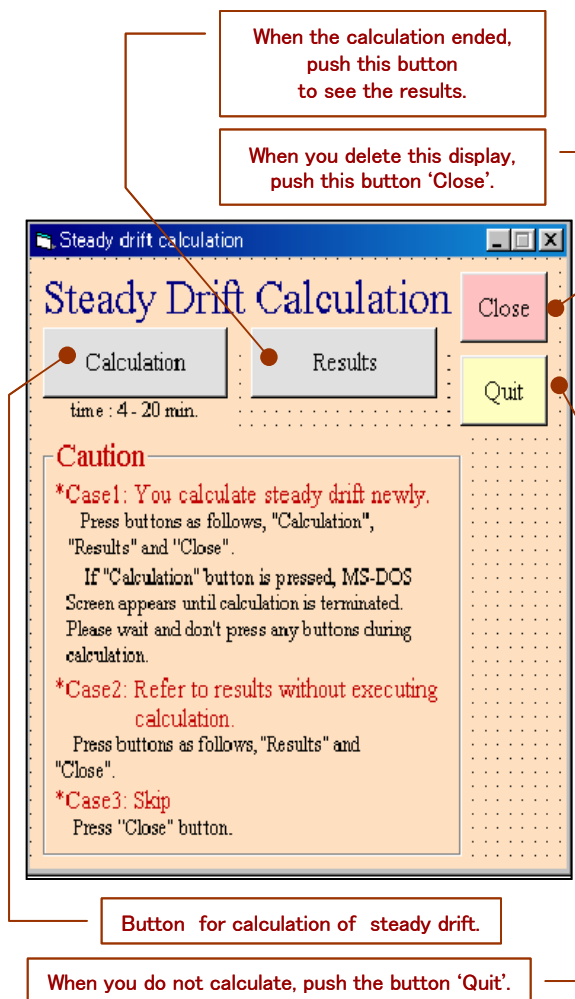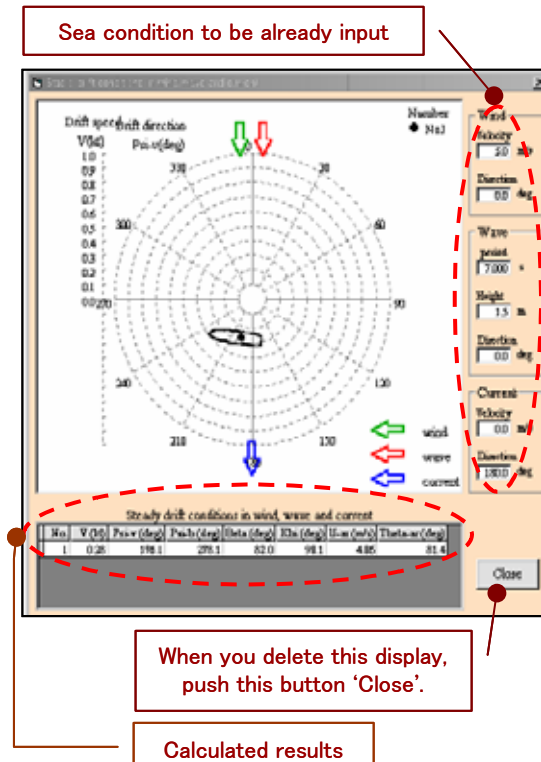

Fig.A17　Display for **'Steady drift calculation'.**

Fig.A18　Display for results of drift.

31

∗ **'Results'** button
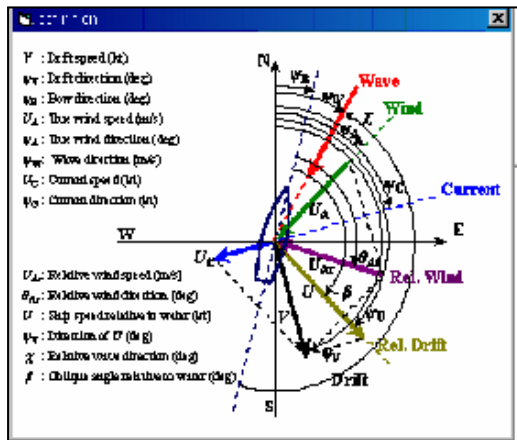
 This is the button for seeing the results of

Fig.A19 Display for definition.

Button for maneuvering simulation

When you delete this display, push this button 'Close'

When you do not calculate, push the button 'Quit'

Button for seeing trajectory

Button for seeing maximum towline tension and unstable motion range.
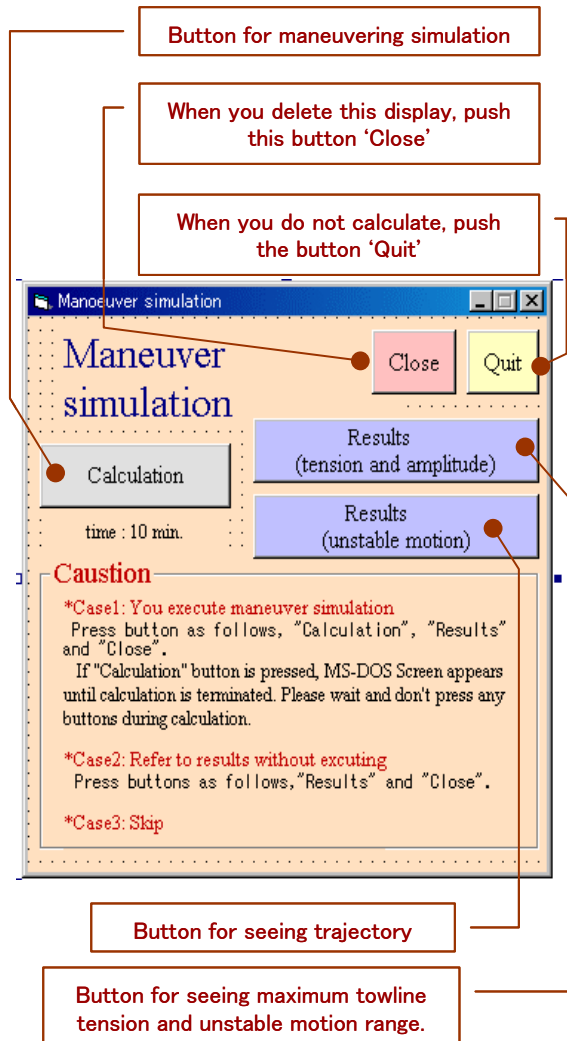
Fig.A20 Display of **'Maneuvering simulation'**

steady drift calculation.

 When you push this button, the following display showing the results of steady drift motion will appear.

Value of solutions(Fig.A18,Fig.A19)

 No. : No. of solution

 V(kt) : Drift speed

 Ψv : Drift direction

 Ψb : Bow direction

(12) Display of **'Maneuver simulation'** (Fig.A20)

 When you select **'New'** on the display of **'input data selection'**, you have to push the button of **'Calculation'**, **'Results'** in order.

 When you select '**Past results**' or '**Default**' on the display of **'input data selection'**, you have only to push the button of **'Simulation results'** instead of pushing **'Calculation'**.

∗ **'Calculation'** button

 When you push this button, the computer program

Towline tension.

Unstable motuin range.

Sea condition already input

When you select the towing speed and push 'Draw' button, graphic display will be drawn

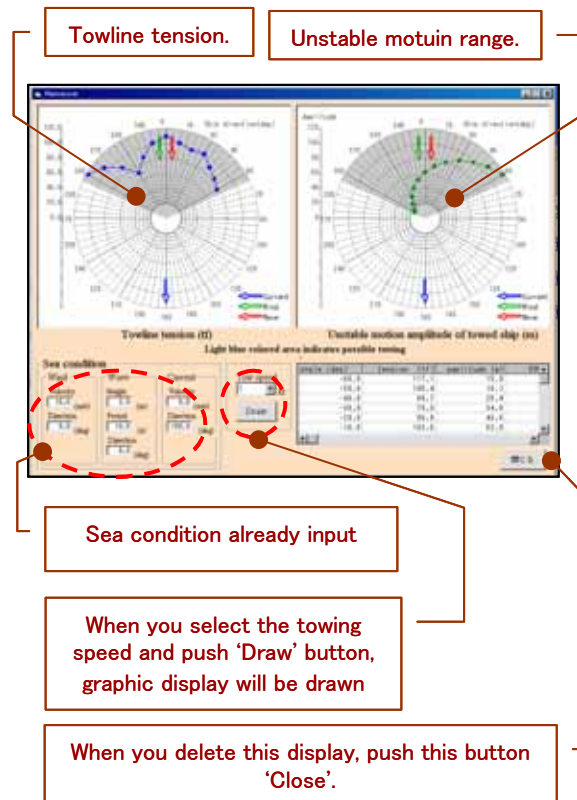When you delete this display, push this button 'Close'.

Fig.A21 Display for results of towline force and unstable motion

32

for calculating the towline tension and trajectory of disabled ships in waves is executed. The display on command prompt will come out. You are not allowed to push **'Simulation results'** button until this display disappears.

∗ **'Simulation results (towline tension and unstable motion range)'** button
    (Fig.A21,Fig.A22)

 This is the button for seeing the results of maximum towline tension and unstable motion range of towed ship. When you push this button, the following graphic display will come out.

(13) Display for **'Save data'** (Fig.A23)
The saved data can be opened from the list of files on the upper left of the display of **'Main'**

∗ **'Save'** button
 When you push this button after input of folder name, all input data and calculation results will be saved.
 When you see the saved results, you select **'Past results'** on the display of Input data selection.

∗ **'Cancel'** button
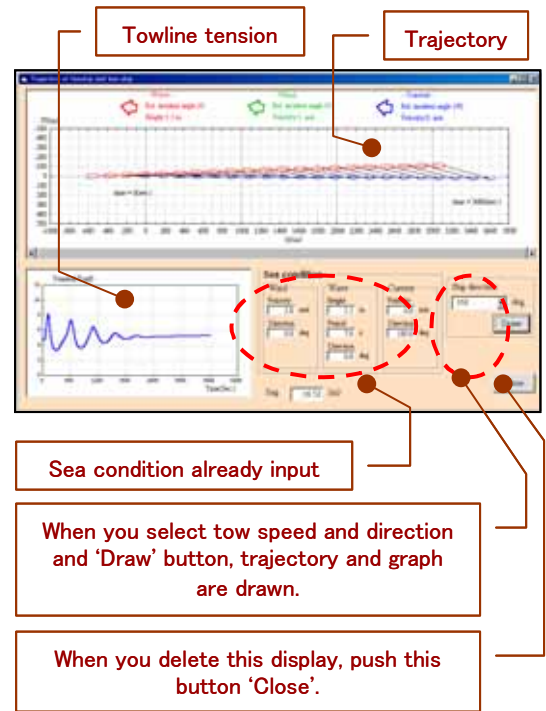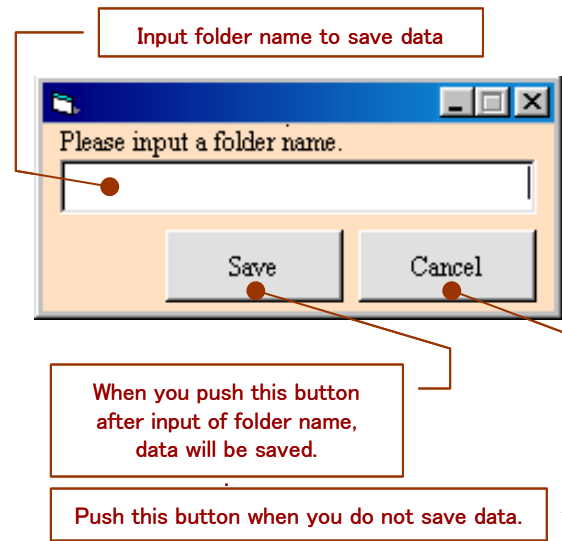 Push this button when you do not save data. The display will disappear.

Fig.A22   Display for trajectory of tow and towed ship

Fig.A23   Display for saving file